Isoscalar and isovector giant resonances in ^{92,94,96,98,100}Mo and ^{90,92,94}Zr

G. Bonasera[1,*], S. Shlomo[1], D.H. Youngblood[1], Y.-W. Lui[1] , Krishichayan[2,3] and J. Button[1]

[1]*Cyclotron Institute, Texas A&M University, College Station, Texas 77843, USA*

[2]*Department of Physics, Duke University, Durham, North Carolina 27708, USA*

[3]*Triangle Universities Nuclear Laboratory, Durham, North Carolina 27708, USA*

(Dated: June 18, 2019)

The response functions, S(E), and centroid energies, E_{CEN}, of the isoscalar and isovector giant resonances of multipolarity L = 0 - 3 in ^{92,94,96,98,100}Mo and ^{90,92,94}Zr have been calculated employing the spherical Hartree-Fock (HF) based random phase approximation (RPA) method, using the Skyrme-type effective nucleon-nucleon interaction. In particular, we investigate the recent experimental results of the uncharacteristic behavior of E_{CEN} for the isoscalar giant resonances, by extending our HF-based RPA calculations with only the KDE0v1 interaction to 32 additional Skyrme interactions. The main result of our investigation is that we find significant disagreements between the theoretical and the experimental values of E_{CEN} for isoscalar giant monopole and dipole resonance of some nuclei. For the isoscalar giant octupole resonance we find the theoretical values of the E_{CEN} to be well above the experimental results. We also study the sensitivity of E_{CEN} to nuclear matter (NM) properties, including the effective mass, the incompressibility coefficient and the symmetry energy at saturation density, by determining the Pearson linear correlation coefficient between the calculated values of E_{CEN} and the various nuclear matter properties of each Skyrme parametrization. For the isovector giant dipole resonance we find good agreement between the experimental and theoretical values of E_{CEN} for Skyrme interactions with values of the enhancement coefficient of the energy weighted sum rule, κ, in the range between 0.25 – 0.70.

* giacomo90@email.tamu.edu

1. INTRODUCTION

Giant resonances in nuclei are collective modes of oscillation of the neutrons against the protons (isovector) or with the protons (isoscalar). The study of these collective modes is fundamental to better constrain the physical properties of nuclear matter (NM) and to understand properties of nuclei as well as properties of the nuclear force. It is common to use these nuclear matter properties to constrain the adopted form of the energy density functional (EDF). One can then study the characteristics of both stable and unstable nuclei, the properties of nuclear structure, astrophysical phenomena and heavy-ion collisions (HIC) [1–3]. To improve our knowledge of EDF, a more accurate value of the NM incompressibility coefficient, K_{NM}, which dictates the curvature of the equation of state of symmetric nuclear matter, is needed, while knowledge of the symmetry energy density, $E_{sym}(\rho)$, is also required for the equation of state of asymmetric NM.

Recently, the isoscalar giant resonances of ^{92,94,96,98,100}Mo [4,5] and ^{90,92,94}Zr [6] have been measured at the Cyclotron Institute of Texas A&M University (TAMU) using inelastic scattering of 240-MeV α particles from the K-500 superconducting cyclotron at small angles, including 0°. Folding model (FM) distorted wave Born approximation (DWBA) calculations of excitation cross sections, using semiclassical transition densities, were carried out to separate the strength functions of the different multi-polarities. Most of the strength of these giant resonances were obtained for the nuclei considered. The strength functions S(E) and the corresponding centroid energies were compared with the results of HF-RPA calculations [4–6] obtained using the KDE0v1 [7] Skyrme-type interaction. Large discrepancies were noted between the measured and calculated centroid energies, E_{CEN}, of the isoscalar giant monopole resonance (ISGMR), isoscalar giant dipole resonance (ISGDR), isoscalar giant quadrupole resonance (ISGQR) and isoscalar giant octupole resonance (ISGOR) of some nuclei. Here we set out to further study these discrepancies by extending our investigation to 32 additional Skyrme interactions. We also compare our calculated results for the ISGMR centroid energies of ^{90,92}Zr and ^{92}Mo with the experimental data from the Research Center for Nuclear Physics (RCNP) at Osaka

University (Osaka, Japan) [8], and find better agreement than with the TAMU data for the ISGMR of ^{92}Mo. For completeness we will also show results for the isovector giant monopole resonance (IVGMR), isovector giant dipole resonance (IVGDR), isovector giant quadrupole resonance (IVGQR) and isovector giant octupole resonance (IVGOR).

Similar to our recent analysis of giant resonances over a wide range of masses [9], in this work we present results of HF-RPA calculations of E_{CEN} for isoscalar (T=0) and isovector (T=1) giant resonances up to L = 3 in ^{92,94,96,98,100}Mo and ^{90,92,94}Zr. The values of E_{CEN} are determined from the strength functions, S(E), obtained within the spherical HF-based RPA method by adopting 33 different parametrizations of the Skyrme effective interaction, and compared to the experimental results. The 33 Skyrme interactions considered are associated with a broad range of values for each nuclear matter property.

In the next section we describe the HF-RPA method for obtaining the centroid energies. In section 3 we present the calculated E_{CEN} for all nuclei for each giant resonance separately and discuss our results. We also analyze the correlation between the calculated values of E_{CEN} and various NM properties by determining the Pearson linear correlation coefficients. In section 4 we give a brief summary and discuss our conclusions.

2. METHOD

Fully self-consistent spherical Hartree-Fock (HF)-based random-phase approximation (RPA) calculations of strength functions, S(E), were performed using 33 different Skyrme interactions commonly employed in the literature. The adopted form of Skyrme effective nucleon-nucleon interaction is taken in the standard form [10]:

$$
\begin{aligned}
V_{ij} = {} & t_0\left(1 + x_0 P_{ij}^{\sigma}\right)\delta\left(\vec{r}_i - \vec{r}_j\right) + \frac{1}{2}t_1\left(1 + x_1 P_{ij}^{\sigma}\right)\left[\overleftarrow{k}_{ij}^{2}\delta\left(\vec{r}_i - \vec{r}_j\right) + \delta\left(\vec{r}_i - \vec{r}_j\right)\vec{k}_{ij}^{2}\right] \\
& + t_2\left(1 + x_2 P_{ij}^{\sigma}\right)\overleftarrow{k}_{ij}\delta\left(\vec{r}_i - \vec{r}_j\right)\vec{k}_{ij} + \frac{1}{6}t_3\left(1 + x_3 P_{ij}^{\sigma}\right)\rho^{\alpha}\left(\frac{\vec{r}_i + \vec{r}_j}{2}\right)\delta\left(\vec{r}_i - \vec{r}_j\right) \\
& + iW_0\overleftarrow{k}_{ij}\delta\left(\vec{r}_i - \vec{r}_j\right)\left(\vec{\sigma}_1 + \vec{\sigma}_2\right) \times \vec{k}_{ij} \, .
\end{aligned}
\tag{1}
$$

Here t_i, x_i, W_0 and α are the 10 Skyrme parameters. P_{ij}^{σ} is the spin exchange operator, while $\vec{\sigma}_i$ is the Pauli spin operator. Also $\vec{k}_{ij} = -\frac{i(\vec{\nabla}_i - \vec{\nabla}_j)}{2}$ and $\overleftarrow{k}_{ij} = -\frac{i(\overleftarrow{\nabla}_i - \overleftarrow{\nabla}_j)}{2}$ are the momentum operators, acting on the right and left, respectively. The Skyrme parameters of a given interaction are commonly obtained by fitting calculations of nuclear properties to different sets of experimental data.

Following the RPA method, the strength function is defined by the sum over all RPA states $|n\rangle$ with energy E_n as:

$$\mathrm{S(E)} = \sum_n |\langle 0|F_{\mathrm{L}}|n\rangle|^2 \delta(E_n - E_0). \qquad (2)$$

The isoscalar (T = 0) single-particle scattering operator is given by $F_L = \sum_i f(r_i) Y_{L0}(i)$, while the isovector (T = 1) single-particle scattering operator is given by $F_L = \frac{Z}{A}\sum_n f(r_n) Y_{L0}(n) - \frac{N}{A}\sum_p f(r_p) Y_{L0}(p)$ [11]. The strength functions of the different multi-polarities are then obtained using: $f(r) = r^2$ for the ISGMR, ISGQR, IVGMR and IVGQR, $f(r) = r^3$ for the ISGOR and IVGOR, $f(r) = r$ for IVGDR, while $f(r) = r^3 - (5/3)\langle r^2\rangle r$ for the ISGDR which removes the contribution of the spurious state [12,13]. We determine the moments, m_k, of the strength function, S(E), and the centroid energy, $\mathrm{E_{CEN}}$, using:

$$m_k = \int_{E_1}^{E_2} E^k \mathrm{S(E)}\, dE \qquad \text{and} \qquad \mathrm{E_{CEN}} = \frac{m_1}{m_0}, \qquad (3)$$

where E_2 - E_1 is the appropriate experimental excitation energy range. Details of the HF-based RPA calculations can be found in Refs. [11–15].

We also investigate the sensitivities of $\mathrm{E_{CEN}}$ of the giant resonances to nuclear matter properties such as the incompressibility coefficient of nuclear matter $\mathrm{K_{NM}}$, the effective mass m*/m, the symmetry energy, E_{sym}, at saturation density, $J = E_{sym}(\rho_0)$, its first derivative, $L = 3\rho_0 \frac{\partial E_{sym}}{\partial \rho}\Big|_{\rho_0}$, and its second derivative, $K_{sym} = 9{\rho_0}^2 \frac{\partial^2 E_{sym}}{\partial \rho^2}\Big|_{\rho_0}$, as well as the enhancement coefficient, κ, of the energy weighted sum rule (EWSR) of the isovector giant dipole resonance (IVGDR). We note that the value of κ for the other multipolarities is very similar to that of the IVGDR, as demonstrated in Ref. [11]. We

quantify these sensitivities using the Pearson linear correlation coefficient, C, which is defined as:

$$C = \frac{\sum_{i=1}^{n}(x_i-\bar{x})(y_i-\bar{y})}{\sqrt{\sum_{i=1}^{n}(x_i-\bar{x})^2}\sqrt{\sum_{i=1}^{n}(y_i-\bar{y})^2}} \quad (4)$$

for quantities x and y, where $\bar{x}$ and $\bar{y}$ are the averages of x and y and the sum runs over all interactions (n = 33). We grade the degree of correlation using the same convention as in Ref. [9]: strong (|C| > 0. 80), medium (|C| = 0.61 – 0.80), weak (|C| = 0.35 – 0.60) and no correlation (|C| < 0.35).

The parameters of the interactions are available in Table I of Ref. [9] for the 33 Skyrme interactions adopted in this work, while in Table II of Ref. [9] we list the conditions defining each interaction (such as the treatment of neutron and proton masses, the Coulomb exchange term, etc.). As can be seen from Table III of Ref. [9], the nuclear matter properties associated with the 33 interactions cover a broad range of values, while in Table V of Ref. [9] we showed the Pearson linear correlation coefficient between pairs of NM properties and found no correlation between any of the NM properties other than between K_{NM} and m*/m, between κ and m*/m, and between J, L, and K_{sym}. For the open shell nuclei we use fractional occupation numbers for the outer orbit thus leaving us with a spherical nucleus while still using all of the interaction terms of the HF calculation for the RPA calculation for self-consistency [16]. It is well known that for open shell spherical nuclei the occupation number approximation provides a good approximation for the response function for excitation energy in the region of giant resonances, see for example Ref. [17] and the online documentation of the TDHF code Sky3D [18]. We add that the difference between the values of the centroid energy obtained by using the occupation number method and by accounting for pairing correlation was estimated in Ref. [19] to be less than 0.3 MeV in this region, which is less than the experimental uncertainty.

The HF-RPA calculations have been carried out for all nuclei in a box of 20 fm and 100 grid points. We ensured that these choices didn't affect our results by also doing the calculation with 200 grid points and same-sized box and then comparing the corresponding energy weighted sum rules and resulting centroid energies. We used 100, 80, 50 and 50

MeV for the maximum cutoff single particle energy for the multipolarities L= 0 - 3, respectively. We also checked our results using a higher cutoff energy and found no significant difference (0.05 MeV, for cutoff energy of 70 MeV for L = 2) in the value of the centroid energies. To ensure accuracy in the values of the centroid energies, the integration in eq. (3) of the energy moments was carried out using a small value of $\Gamma = 0.1$ MeV for the width of the Lorentzian smearing applied to the discrete strength distribution, S(E). Also, to determine the energy moments of the strength function we integrate over the same energy range used to determine the experimental data for the centroid energy, in order to make a proper comparison. The energy ranges are 9-36 MeV for the ISGMR and ISGQR, 20-36 MeV for (the high energy component of) the ISGDR, and 15-36 MeV for the ISGOR. Notice that the integration range for the ISGDR and the ISGOR were started at higher energy than for the other resonances so that the low energy peak is not taken into the integral. For the isovector resonances we used the following energy ranges: 15-60 MeV for the IVGMR and the IVGQR, 0-60 MeV for the IVGDR, and 22-60 MeV for the IVGOR.

3. RESULTS

In the following we present our main results of HF-RPA calculations of the centroid energies, E_{CEN}, of the isoscalar and isovector giant resonances of multipolarity L = 0-3 in ^{92,94,96,98,100}Mo and ^{90,92,94}Zr, using the 33 Skyrme-type interactions shown in Tables I and II of Ref. [9]. We discuss the dependence of E_{CEN} on NM properties and compare with available experimental data, shown in Table I. In Table II we show the calculated Pearson linear correlation coefficient, C, between each E_{CEN} and various NM properties. It is important to note the similarity between the values of C in this work and the values calculated for a wide range of nuclei from ^{40}Ca to ^{208}Pb shown in Table VI of Ref. [9]. We also explore the effect of increasing the neutron or proton number on the centroid energy by comparing E_{CEN} of giant resonances of neighboring isotopes and isotones, using the isospin asymmetry coefficient $I = \frac{N-Z}{A}$. In Appendix A we present Tables for the values of: the nuclear matter properties, and the resulting centroid energies for the isoscalar and isovector giant resonances associated with the 33 Skyrme interactions used in the calculations.

3.1 Isoscalar giant monopole resonance

In FIG. 1 we plot the centroid energy E_{CEN} of the isoscalar giant monopole resonance (ISGMR), calculated within the spherical HF-based RPA method described above, against the nuclear matter incompressibility coefficient, K_{NM}, associated with the interaction used for the calculation. Every isotope is considered individually with its respective experimental data, obtained at the Cyclotron Institute at Texas A&M University (TAMU), marked by the dashed lines. The solid lines represent the data obtained at the Research Center for Nuclear Physics (RCNP), Osaka University, Osaka, Japan (Osaka) [8], shown only for ^{92}Mo since the results of Osaka for the ^{90,92}Zr isotopes are very close to the TAMU results. In agreement with the literature we obtain a strong correlation for the calculated values of E_{CEN} to K_{NM} [20–24], with a Pearson linear correlation coefficient of C ~ 0.87. Despite the strong correlation with the incompressibility coefficient, we can't make tight constraints on the value of K_{NM} due to the disagreement between the experimental data and the theoretical predictions. This is in contrast with our work with closed shell nuclei ranging from ^{40}Ca to ^{208}Pb where we determined an optimal range for K_{NM} between 210 and 240 MeV [9]. Considering the TAMU experimental values of E_{CEN} for the ISGMR we find in the case of ^{92}Mo an agreement with the theoretical results for interaction associated with a value of K_{NM} greater than 260 MeV. For ^{94}Zr, interactions with values of K_{NM} less than 200 MeV would be needed to reproduce the experimental result, while for ^{96}Mo and ^{90,92}Zr we obtain agreement for interactions with values of K_{NM} in the range of 210 - 240 MeV. Meanwhile none of the values of E_{CEN} associated with the interactions considered agree with the experimental values for the most neutron rich nuclei ^{98,100}Mo and ^{94}Zr, with the theoretical value consistently above the experimental value. A weak correlation is found between the calculated values of E_{CEN} and effective mass (C ~ -0.51). No correlation is found between E_{CEN} and the symmetry energy coefficient at saturation density ρ_0, $J = E_{sym}[\rho_0]$ (C ~ -0.05). We find similar results for its first derivative L, and weak correlation for its second derivative K_{sym} (C ~ 0.42). Note that, as mentioned

earlier, the NM matter properties, J, L and K_{sym} are correlated.

For the ISGMR, the change in the centroid energy, $\Delta E_{CEN} = E_{CEN}(I_0) - E_{CEN}(I)$, is plotted against the isospin asymmetry coefficient, I = (N-Z)/A, in FIG. 2a and FIG. 2b. The figure shows a smaller value of E_{CEN} for increasing I in the experimental and theoretical results. However, it is important to point out that the variation in the experimental results of E_{CEN} with I is not reproduced by the theory [25]. In particular, the centroid energies of ^{92}Zr and ^{92}Mo experimentally obtained by the Texas A&M group were above that of ^{90}Zr by 0.35 and 1.74 MeV, respectively. In the theory only the SKO interaction yields a higher E_{CEN} for ^{92}Mo than for ^{90}Zr, while all interactions predict the values of the two Zr isotopes to be practically identical.

3.2 Isoscalar giant dipole resonance

In FIG. 3 we show the centroid energy, E_{CEN}, of the ISGDR plotted against the nuclear matter incompressibility coefficient, K_{NM}. Each isotope is considered separately; the experimental value of the centroid energy is demarcated by dashed lines. We obtained a weak correlation for the calculated values of E_{CEN} and the incompressibility coefficient, K_{NM} (C ~ 0.53). A strong correlation is instead obtained for the calculated values of E_{CEN} and the effective mass, m*/m, (C = -0.91). However, we cannot set limits on the range of m*/m because the different isotopes point to different values of m*/m: the experimental centroid energy of ^{96,100}Mo and ^{92}Zr agrees with the E_{CEN} calculated using the interactions with the lowest value of the effective mass around 0.6, while the E_{CEN} for the rest of the nuclei agrees with the result obtained from interactions associated with m*/m between 0.8 and 1.0. No correlation is found for J and the centroid energy (C ~ -0.07) or with its first derivative, L, while for its second derivative, K_{sym}, we obtain weak correlation (C ~ 0.37). Thus, we cannot make any constraints on these properties.

We add that, in the case of the Mo isotopes, the position of E_{CEN} as a function of

the asymmetry coefficient, I, follows a seesaw in the experimental data while for all the interactions considered here the calculated centroid energy is predicted to decrease as the neutron number is increased as FIG. 2c shows. For the Zr isotopes we show in FIG. 2d that the experimental data again shows a seesaw trend with ^{94}Zr having the highest centroid energy. Conversely, we find the overall trend for the interactions considered here is that the centroid energy decreases as the neutron number is increased, in agreement with the calculated results for the Mo isotopes. These experimental fluctuations are not seen for closed shell nuclei across a wide range of masses, where we find instead that the experimental result is consistently below the theoretical calculations [9].

3.3 Isoscalar giant quadrupole resonance

The centroid energies of the isoscalar giant quadrupole resonance (ISGQR) obtained from the HF-RPA, from the various interactions considered, are plotted as full circles against the effective mass, m*/m, in FIG. 4. Similarly to what was found in Refs. [9,14], the calculated values of the centroid energy of the ISGQR shows a strong correlation with the effective mass (C ~ -0.96). In particular, when comparing with experimental data, the Mo isotopes with more neutrons prefer a higher effective mass, while the Zr isotopes show the opposite trend. However, we find that for all nuclei the experimental values of E_{CEN} are close to the theoretical values for interactions with an effective mass between 0.8 and 0.9, in agreement with our results obtained from the ISGQR of closed shell nuclei ranging from ^{40}Ca to ^{208}Pb [9]**.** In the case of the incompressibility coefficient, K_{NM}, we obtain a weak correlation between the values of K_{NM} and E_{CEN} (C ~ 0.37). In the case of the symmetry energy coefficient, *J*, and its first derivative, *L,* no correlation is obtained with the centroid energy for the isotopes considered here, while for the second derivative, K_{sym}, a weak correlation is obtained with E_{CEN} (C ~ 0.41).

Considering the E_{CEN} of all the nuclei together plotted against the asymmetry coefficient, I, we obtain a decreasing centroid energy as I is increased in both the experimental and the theoretical values, as seen in FIG. 2e and FIG. 2f. However, the ^{94}Zr isotope breaks this trend and the experimental value of E_{CEN} is found to be above those of

its neighboring nuclei, while in the results of the calculations it has the lowest centroid energy for all the interactions.

3.4 Isoscalar giant octupole resonance

In FIG. 5 we show with full circles centroid energies E_{CEN} of the isoscalar giant octupole resonance (ISGOR), obtained from the HF-RPA, as a function of the effective mass, m*/m. The experimental data is marked by the dashed lines. A strong correlation (C = -0.98) is obtained for E_{CEN} and m*/m. It is seen from FIG. 5 that generally the theory predicts that the centroid energy is higher than the corresponding experimental value, similar to our findings in Ref. [9] which covered several closed-shell nuclei. Only the experimental values of E_{CEN} for ^{92,94}Zr agree with theory for a few interactions with large m*/m ≈ 1 (mostly the SkT series). A weak correlation (C = 0.39) is obtained between the incompressibility coefficient of nuclear matter, K_{NM}, and the centroid energy. For the symmetry energy density properties *J* and *L* we find no correlation with the centroid energy of the isotopes considered here, while for K_{sym} we obtain weak correlation with E_{CEN} (C = 0.38).

The calculated centroid energy of the Mo isotopes shows a clear decreasing trend as the mass (and I) increases. A similar pattern is seen in the experimental result, however the centroid energy of ^{94}Mo breaks this trend and was measured 3 MeV above the other isotopes. As shown in FIG. 2g no interaction predicts this behavior. All interactions predict the centroid energy to be higher in ^{94}Mo than in ^{96}Mo, with up to 1.4 MeV difference in a few cases. For the case of the Zr isotopes our calculations show in FIG. 2h a similar trend to the Mo isotopes, with the values of E_{CEN} decreasing as the mass increases. However, all the interactions predict the centroid energy of the ^{94}Zr isotope to be significantly higher than the experimental result.

3.5 Isovector giant monopole resonance

No experimental data for E_{CEN} of the isovector giant monopole resonance (IVGMR) is available for the nuclei studied here. We show the results of the HF-RPA calculations for E_{CEN} in FIG. 6, plotted against K_{NM}. Although this is a compression mode, no correlation is obtained between E_{CEN} and K_{NM} (C = 0.25). Conversely, medium correlation is obtained between the calculated centroid energy and the effective mass m^*/m (C ~ -0.71). We show in FIG. 7 E_{CEN} plotted against the symmetry energy coefficient *J.* No correlation is obtained for the symmetry energy and the centroid energy (C ~ -0.24) for this isovector giant resonance. Similar results are obtained for the derivatives of the symmetry energy, L and K_{sym} (C < 0.10 in both cases). We find a strong dependence of the centroid energy of the IVGMR on the IVGDR energy weighted sum rule enhancement coefficient κ (C ~ 0.85). In FIG. 8a and FIG. 8b we analyze the result of our calculation for E_{CEN} of these nuclei plotted against the asymmetry coefficient, I, and we find that the theory predicts smaller centroid energies as the system becomes more neutron rich.

3.6 Isovector giant dipole resonance

In FIG. 9 the E_{CEN} of the isovector giant dipole resonance (IVGDR) resulting from the HF-RPA calculations is plotted against the symmetry energy coefficient, *J*. Experimental data of the centroid energy is available for all the isotopes of Mo [26] and Zr [27] considered here and is marked by the dashed lines. This is a well-studied resonance, with experimental data established in the 1970s, and as expected we find that for all the nuclei considered here our calculations agree with the experimental result. We point out that for this isovector giant resonance a weak correlation was obtained between the centroid energy and the symmetry energy coefficient J (C ~ -0.35) and its first derivative L (C ~ -0.39), while no correlation is found for the second derivative K_{sym} (C ~ -0.29), similar to the results of Refs. [9,14]. We demonstrate in FIG. 10 a strong correlation between E_{CEN} and the IVGDR energy weighted sum rule enhancement coefficient κ (C ~ 0.85). We find that the interactions with κ between 0.25 to 0.7 are the closest to the experimental measurement. This is in good agreement with our previous work of extracting κ for closed shell nuclei between ^{40}Ca and ^{208}Pb [9]. A medium correlation was obtained

for the calculated values of E_{CEN} with the effective mass, m*/m, (C ~ -0.61). We also point out that there is a medium correlation (C ~ -0.63) between the effective mass and κ. In FIG. 8c and FIG. 8d, we show that the theoretical and the experimental results for E_{CEN} decrease with an increasing value of the asymmetry coefficient I, for both the Mo and Zr isotopes, respectively.

3.7 Isovector giant quadrupole resonance

For the isovector giant quadrupole resonance (IVGQR) there is no available experimental data for E_{CEN}. For this isovector excitation we show in FIG. 11 that no correlation exists between the values of E_{CEN} and the first derivative of the symmetry energy coefficient, *L,* (C ~ -0.27). Similarly, no correlation was obtained for the symmetry energy coefficient, *J*, (C ~ -0.34) or its second derivative, K_{sym}, (C ~ -0.11). We find a strong correlation for the calculated E_{CEN} of the IVGQR and the IVGDR energy weighted sum rule enhancement coefficient κ (C ~ 0.85). Lastly, we report a medium correlation (C ~ -0.77) of the centroid energy on the effective mass, as shown in FIG. 12. We look at the Mo and Zr isotope chains individually in FIG. 8e and 18f, respectively. As expected, we obtained a decreasing value of the calculated E_{CEN} as I is increased.

3.8 Isovector giant octupole resonance

For the isovector giant octupole resonance (IVGOR) no measurements of E_{CEN} are available. Our calculated results for the centroid energy are shown in FIG. 13, plotted against the second derivative of the symmetry energy coefficient, K_{sym}. The two sets of calculated values, E_{CEN} and K_{sym}, are not correlated (C ~ 0.02) for this isovector giant resonance. Similar results were found for the symmetry energy coefficient, *J*, (C ~ -0.28) and its first derivative, *L,* (C ~ -0.18). A strong correlation is obtained between E_{CEN} and the IVGDR energy weighted sum rule enhancement coefficient κ (C ~ 0.83). We show in FIG. 14 the E_{CEN} plotted against m*/m. As can be seen from the figure, we obtained a strong correlation between the calculated E_{CEN} and m*/m (C ~ -0.86) for all the isotopes

considered.

We study the centroid energies for Mo and Zr isotopes in FIG. 8g and FIG. 8h, respectively, by showing E_{CEN} as a function of the asymmetry coefficient I. For the Mo isotopes we find that the position of the centroid energy decreases as the mass increases, with the results obtained from Sly4 and SLy5 deviating slightly for the cases of ^{98}Mo and ^{100}Mo. Similarly, for the Zr isotopes, we obtained a decreasing centroid energy as the mass increases for all interactions.

4. SUMMARY AND CONCLUSIONS

Results of HF-RPA calculations of centroid energies, E_{CEN}, for the isoscalar and isovector excitations up to L = 3 in ^{92,94,96,98,100}Mo and ^{90,92,94}Zr isotopes were presented and compared with experimental data. The calculations were performed for 33 different Skyrme-type effective interactions of the standard form (see Table I of Ref. [9] for details). We also investigated the correlation between E_{CEN} and the nuclear matter properties associated with each Skyrme interaction. As shown in Fig.1 of Ref. [9], a large range of values for each nuclear matter property is covered by our choice of Skyrme interactions. Among pairs of NM properties we found some correlations between the incompressibility coefficient, K_{NM} and m*/m, between κ and m*/m, and between the symmetry energy coefficient and its derivatives while no correlation (i.e. $|C| < 0.35$) is found for the remaining pairs of NM properties, see Table V of Ref. [9] for the exact values of C.

The main result of this investigation is that the disagreement between the experimental result and the HF-based RPA calculations of E_{CEN} [4–6], obtained using the KDE0v1 interaction [7], are also present for the other 32 interactions considered in this work. The experimental values of E_{CEN}, measured at the Cyclotron Institute at Texas A&M University (TAMU), for the isoscalar giant monopole resonance (ISGMR) in ^{92}Zr and ^{92}Mo are higher than the measured value of E_{CEN} of ^{90}Zr by 0.35 and 1.74 MeV, respectively, in disagreement with the theoretical result. On the other hand, the experimental values of

E_{CEN}, measured at the Research Center for Nuclear Physics (RCNP) at Osaka University (Osaka, Japan) by Gupta et al. [8], follow the expected decreasing value of E_{CEN} as the mass increases, and the value of the E_{CEN} of ^{92}Mo is found to be in agreement with interactions with a value of the incompressibility coefficient, K_{NM}, from 210 to 240MeV. However, in a more recent publication by the same authors [28], they report significantly higher values for the E_{CEN} of ^{90,92}Zr and ^{92}Mo than what was previously stated in Ref. [8]. This new result, while still obeying the decreasing trend of the centroid energy as the mass is increased, points to a value for K_{NM} above 250 MeV. For the most neutron rich isotopes considered here, namely ^{94}Zr, and ^{98,100}Mo, we find that for all of the 33 interactions used in this work the values of E_{CEN} are significantly above the corresponding experimental values. For the isoscalar giant dipole resonance (ISGDR) the calculated values of E_{CEN} for ^{96,100}Mo and ^{92}Zr are smaller than the experimental result, while in the case of ^{92,94,98}Mo and ^{90,94}Zr the calculated E_{CEN} are larger than the corresponding experimental data, for most of the interactions used. For the isoscalar giant quadrupole resonance (ISGQR) we find that the calculated E_{CEN} agrees with the experimental measurement for most Skyrme parametrizations. This is not the case for the isoscalar giant octupole resonance (ISGOR), in which the experimental values for E_{CEN} are significantly smaller than the calculated values. These disagreements are clearly seen as fluctuations when we consider the variations of E_{CEN} with the asymmetry coefficient, $I = (N - Z)/A$. For the isovector giant resonances, experimental data for E_{CEN} is only available for the isovector giant dipole resonance (IVGDR) of the ^{92,94,96,98,100}Mo and ^{90,92,94}Zr isotopes. For the IVGDR, the results of the HF-RPA calculations reproduce the experimental measurement for quite a few interactions.

We have also studied the sensitivities of the calculated values of E_{CEN} of the various giant resonances to the values of nuclear properties related to the 33 Skyrme parametrizations adopted in the HF-RPA calculations by evaluating the relative Pearson linear correlation coefficient, C, shown in Table II, and obtained results very similar to those obtained in our previous work concerning spherical nuclei, see Table VI of Ref. [9]. A strong correlation is obtained for the calculated E_{CEN} and the incompressibility coefficient, K_{NM}, for the ISGMR and for E_{CEN} and m*/m for all the isoscalar giant resonances studied. However, due to the disagreement between experimental data and

theoretical values of E_{CEN}, it is not possible to determine the values of K_{NM} and m*/m within reasonable accuracy. We obtain a very weak correlation for the values of E_{CEN} resulting from the HF-RPA and the values of the symmetry energy coefficients, *J*, *L,* and K_{sym}. On the other hand, there are strong correlations between the value of κ, the enhancement coefficient for the energy weighted sum rule of the isovector giant dipole resonance, and centroid energies for the isovector giant resonances resulting from the HF-RPA. Therefore, using the available data for the centroid energies of the IVGDR, we can suggest that the value of κ is between 0.25 and 0.7, in agreement with our previous results obtained for a wide range of spherical nuclei [9].

The discrepancy between the theoretical and the experimental values of E_{CEN} for the isotopes of Mo and Zr nuclei is still an unresolved problem which calls for further investigations, such as: (i) use of calculated HF-based RPA microscopic transition densities in the analysis of the experimental excitation cross-section data [12,29] instead of the semi-classical transition densities that were used in the analyses of the experimental data within the folding-model distorted wave Born approximation, and; (ii) carry out calculations beyond the mean-field approximation by including nuclear structure effects [30–36].

ACKNOWLEDGEMENT

Funding: This work was supported in part by the US Department of Energy under Grant No. DE-FG03-93ER40773.

APPENDIX A

Table A1 Values of NM properties associated with the Skyrme interactions (see Table I of Ref. [9] for details). We have the saturation density ρ_0 [$^{fm-3}$], the total binding energy per nucleon E/A [MeV], the incompressibility coefficient K_{NM} [MeV] of NM, the coefficients related to the symmetry energy density J [MeV], L [MeV] and K_{sym} [MeV], the isoscalar effective mass m*/m, the enhancement factor of the EWSR of the IVGDR κ, the Landau parameter G_0' and the strength of the spin-orbit interaction W_0 (MeV).

Force	ρ_0	E/A	K_{NM}	J	L	K_{sym}	m*/m	κ	W_0	G_0'
SGII	0.159	15.59	215.0	26.80	37.63	-145.90	0.79	0.49	105.00	0.5052
KDE0	0.161	16.11	228.8	33.00	45.22	-144.78	0.72	0.30	128.96	0.0474
KDE0v1	0.165	16.23	227.5	34.58	54.70	-127.12	0.74	0.23	124.41	0.0006
SKM*	0.160	15.78	216.7	30.03	45.78	-155.94	0.79	0.53	130.00	0.3142
SK255	0.157	16.33	255.0	37.40	95.00	-58.33	0.80	0.54	95.39	0.3733
SkI3	0.158	15.96	258.1	34.80	100.52	73.04	0.58	0.25	188.51	0.2035
SkI4	0.160	15.92	247.9	29.50	60.39	-40.56	0.65	0.25	366.19	1.3813
SkI5	0.156	15.83	255.7	36.70	129.33	159.57	0.58	0.25	123.63	0.3013
SV-bas	0.160	15.90	234.0	30.00	45.21	-221.75	0.90	0.40	124.63	0.7279
SV-min	0.161	15.91	222.0	30.01	44.76	-156.57	0.95	0.08	111.29	0.7963
SV-sym32	0.159	15.94	233.81	32.00	57.07	-148.79	0.90	0.40	132.745	0.8319
SV-m56-O	0.157	15.81	254.6	27.00	49.96	-45.04	0.56	0.60	133.27	1.6523
SV-m64-O	0.159	15.82	241.4	27.01	30.63	-144.76	0.64	0.60	113.97	1.4667
SLy4	0.160	15.97	229.9	32.00	45.96	-119.73	0.70	0.25	123.00	-0.1337
SLy5	0.160	15.98	229.9	32.03	48.27	-112.76	0.70	0.25	126.00	-0.1414
SLy6	0.159	15.92	229.8	31.96	47.44	-112.71	0.69	0.25	122.00	-0.0038
SkMP	0.157	15.56	230.9	29.88	70.31	-49.82	0.65	0.71	160.00	0.4653
SkO	0.160	15.84	223.34	31.97	79.14	-43.17	0.90	0.17	353.16	1.6191
SkO'	0.160	15.75	222.3	31.95	68.93	-78.82	0.90	0.15	287.79	0.7923
LNS	0.175	15.32	210.78	33.43	61.45	-127.36	0.83	0.38	96.00	0.1367
MSL0	0.160	16.00	230.00	30.00	60.00	-99.33	0.80	0.43	133.30	0.4160
NRAPR	0.161	15.85	225.65	32.78	59.63	-123.32	0.69	0.66	41.96	0.4100
SQMC650	0.172	15.57	218.11	33.65	52.92	-173.15	0.78	0.59	110.5	0.2018
SQMC700	0.171	15.49	222.20	33.47	59.06	-140.84	0.76	0.56	104.60	0.3600
SkT1	0.161	15.98	236.16	32.02	56.18	-134.83	1.00	0.00	110.00	0.1642
SkT2	0.161	15.94	235.73	32.00	56.16	-134.67	1.00	0.00	120.00	0.1573
SkT3	0.161	15.95	235.74	31.50	55.31	-132.05	1.00	0.00	126.00	0.4516
SkT8	0.161	15.94	235.70	29.92	33.72	-187.52	0.83	0.20	109.00	0.2386
SkT9	0.160	15.88	234.91	29.76	33.74	-185.62	0.83	0.20	130.00	0.2142
SkT1*	0.162	16.20	238.95	32.31	56.58	-136.66	1.00	0.00	95.00	0.1757
SkT3*	0.162	16.20	238.95	31.97	56.32	-133.65	1.00	0.00	95.00	0.4616
Skxs20	0.162	15.79	201.76	35.49	67.07	-122.25	0.96	0.08	162.73	0.1286
Z_σ	0.163	15.88	233.33	26.69	-29.38	-401.43	0.78	0.51	123.69	0.3951

Table A2 Calculated centroid energies (in MeV) for the ISGMR.

ISGMR	^{92}Mo	^{94}Mo	^{96}Mo	^{98}Mo	^{100}Mo	^{90}Zr	^{92}Zr	^{94}Zr
SGII	18.03	18.11	17.27	17.35	17.21	17.89	17.96	17.06
KDE0	18.20	18.28	17.50	17.53	17.31	17.96	18.03	17.23
KDE0v1	18.19	18.24	17.45	17.51	17.26	17.97	18.04	17.21
SKM*	17.77	17.91	17.05	17.09	16.94	17.61	17.73	16.83
Sk255	18.86	18.93	18.00	18.17	17.90	18.73	18.79	17.97
SkI3	19.89	19.87	18.80	18.80	18.69	19.57	19.56	18.64
SkI4	19.17	19.19	18.42	18.36	18.04	18.93	18.93	18.12
SkI5	19.35	19.37	18.56	18.34	18.27	19.14	19.11	18.28
SV-bas	18.43	18.58	17.67	17.68	17.54	18.32	18.45	17.66
SV-min	17.96	18.09	17.25	17.27	17.15	17.83	17.95	17.12
SV-sym32	18.42	18.55	17.69	17.66	17.51	18.27	18.41	17.62
SV-m56-O	19.46	19.45	18.65	18.58	18.33	19.18	19.17	18.34
SV-m64-O	18.92	18.94	17.98	17.96	17.91	18.68	18.75	17.94
SLy4	17.90	17.92	17.21	17.24	17.04	17.69	17.72	16.96
SLy5	18.14	18.16	17.24	17.22	17.23	17.93	17.95	17.16
SLy6	18.31	18.36	17.44	17.47	17.38	18.13	18.20	17.40
SkMP	18.49	18.56	17.68	17.73	17.56	18.26	18.32	17.37
SKO	17.52	17.60	16.85	16.84	17.03	17.58	17.70	16.87
SKO`	17.90	18.00	17.26	17.28	17.18	17.79	17.87	17.13
LNS	18.35	18.43	17.48	17.54	17.42	18.20	18.25	17.42
MSL0	18.02	18.13	17.27	17.27	17.19	17.88	17.98	17.08
NRAPR	17.77	17.77	17.09	17.10	17.17	17.67	17.65	16.89
SQMC650	17.76	17.93	17.04	17.07	16.91	17.60	17.71	16.75
SQMC700	18.38	18.49	17.56	17.62	17.42	18.20	18.31	17.47
SkT1	18.32	18.43	17.59	17.56	17.47	18.19	18.31	17.56
SkT2	18.34	18.45	17.61	17.59	17.47	18.21	18.30	17.57
SkT3	18.28	18.40	17.55	17.51	17.43	18.21	18.29	17.54
SkT8	18.39	18.46	17.54	17.59	17.48	18.25	18.33	17.50
SkT9	18.32	18.49	17.56	17.51	17.47	18.19	18.31	17.51
SkT1*	18.13	18.24	17.37	17.58	17.29	18.03	18.15	17.38
SkT3*	18.14	18.24	17.38	17.53	17.29	18.09	18.18	17.43
Skxs20	17.17	17.30	16.49	16.50	16.29	16.96	17.04	16.36
Z-sigma	18.61	18.69	17.64	17.71	17.60	18.44	18.52	17.61
Exp.	19.62	17.99	16.95	16.01	16.13	17.88	18.23	16.16
Error	0.28	0.72	0.12	0.19	0.11	0.12	0.14	0.115

Table A3 Calculated centroid energies (in MeV) for the ISGDR.

ISGDR	^{92}Mo	^{94}Mo	^{96}Mo	^{98}Mo	^{100}Mo	^{90}Zr	^{92}Zr	^{94}Zr
SGII	28.54	28.53	27.86	27.76	27.69	28.35	28.34	27.94
KDE0	28.95	28.81	28.53	28.50	28.46	28.84	28.72	28.39
KDE0v1	28.81	28.70	28.37	28.36	28.37	28.69	28.56	28.27
SKM*	28.10	28.13	27.43	27.37	27.22	27.86	27.73	27.47
Sk255	28.71	28.62	28.29	28.17	28.22	28.66	28.51	28.27
SkI3	29.72	29.84	29.69	29.32	29.26	29.41	29.30	29.31
SkI4	29.49	29.58	29.37	29.31	29.35	29.09	29.15	29.00
SkI5	29.71	29.65	29.56	29.50	29.27	29.40	29.24	29.25
SV-bas	28.14	28.20	27.74	27.65	27.59	28.07	27.98	27.63
SV-min	27.61	27.67	27.33	27.26	27.07	27.49	27.52	27.15
SV-sym32	28.11	28.15	27.74	27.62	27.50	28.01	27.92	27.57
SV-m56-O	29.67	29.81	29.67	29.51	29.45	29.56	29.56	29.56
SV-m64-O	29.58	29.49	29.15	29.03	29.09	29.29	29.19	29.02
SLy4	28.60	28.48	28.16	28.19	28.21	28.53	28.42	28.12
SLy5	28.81	28.67	28.41	28.42	28.40	28.63	28.62	28.33
SLy6	29.09	28.97	28.66	28.46	28.24	28.85	28.66	28.32
SkMP	29.03	29.14	28.26	28.27	28.32	28.77	28.73	28.42
SKO	27.50	27.47	27.09	27.00	27.07	27.60	27.52	27.38
SKO`	27.92	27.97	27.69	27.49	27.22	27.85	27.84	27.45
LNS	28.96	28.95	28.56	28.51	28.40	28.83	28.79	28.30
MSL0	28.12	28.18	27.70	27.79	27.45	27.91	27.91	27.55
NRAPR	29.00	28.81	28.45	28.34	28.48	28.83	28.63	28.20
SQMC650	28.16	28.11	27.58	27.55	27.29	27.92	27.83	27.52
SQMC700	28.84	28.99	28.56	28.56	28.39	28.70	28.64	28.33
SkT1	27.50	27.54	27.27	27.15	27.08	27.58	27.60	27.39
SkT2	27.53	27.55	27.30	27.18	27.09	27.56	27.60	27.37
SkT3	27.47	27.49	27.35	27.26	27.10	27.55	27.65	27.35
SkT8	28.23	28.18	27.83	27.77	27.84	28.35	28.20	27.83
SkT9	28.19	28.20	27.82	27.81	27.84	28.17	28.04	27.75
SkT1*	27.53	27.55	27.29	27.22	27.15	27.46	27.53	27.19
SkT3*	27.45	27.46	27.22	27.14	27.11	27.39	27.51	27.19
Skxs20	27.28	27.23	26.85	26.71	26.59	26.95	26.91	26.52
Z-sigma	28.91	28.82	28.50	28.58	28.49	28.87	28.77	28.27
Exp.	27.60	26.50	30.00	27.40	30.10	27.40	30.00	27.00
Error	0.50	0.43	0.70	0.70	0.70	0.50	0.70	0.50

Table A4 Calculated centroid energies (in MeV) for the ISGQR.

ISGQR	^{92}Mo	^{94}Mo	^{96}Mo	^{98}Mo	^{100}Mo	^{90}Zr	^{92}Zr	^{94}Zr
SGII	15.04	15.02	14.35	14.34	14.31	14.86	14.83	14.18
KDE0	15.56	15.55	14.90	14.88	14.87	15.38	15.41	14.67
KDE0v1	15.44	15.44	14.78	14.77	14.76	15.27	15.28	14.56
SKM*	14.86	14.93	14.32	14.32	14.21	14.70	14.76	14.13
Sk255	14.63	14.65	13.93	13.89	13.92	14.46	14.45	13.75
SkI3	17.66	17.59	16.38	16.41	16.27	17.37	17.34	16.09
SkI4	16.45	16.41	15.63	15.60	15.52	16.15	16.22	15.39
SkI5	17.11	17.05	16.17	16.13	16.08	16.88	16.86	15.89
SV-bas	14.29	14.29	13.67	13.68	13.66	14.06	14.15	13.49
SV-min	13.92	13.98	13.44	13.35	13.34	13.76	13.75	13.20
SV-sym32	14.19	14.20	13.65	13.59	13.55	14.06	14.05	13.45
SV-m56-O	17.50	17.52	16.62	16.57	16.53	17.21	17.28	16.36
SV-m64-O	16.50	16.58	15.75	15.77	15.69	16.24	16.32	15.51
SLy4	15.41	15.43	14.77	14.77	14.76	15.20	15.22	14.56
SLy5	15.46	15.52	14.79	14.85	14.84	15.27	15.29	14.56
SLy6	15.84	15.83	15.13	15.13	15.10	15.66	15.67	14.93
SkMP	16.07	16.06	15.13	15.12	15.00	15.82	15.89	14.87
SKO	13.75	13.79	13.24	13.13	13.14	13.64	13.68	13.11
SKO`	14.11	14.13	13.56	13.45	13.46	14.02	14.02	13.32
LNS	15.63	15.62	14.96	14.93	14.85	15.46	15.44	14.74
MSL0	14.70	14.78	14.08	14.02	14.04	14.58	14.57	13.90
NRAPR	15.25	15.22	14.57	14.51	14.59	15.10	15.08	14.38
SQMC650	15.10	15.20	14.46	14.45	14.33	14.94	14.96	14.18
SQMC700	15.74	15.76	14.89	14.92	14.77	15.57	15.56	14.69
SkT1	13.49	13.52	12.93	12.86	12.92	13.25	13.36	12.72
SkT2	13.50	13.60	13.03	12.96	12.94	13.37	13.38	12.77
SkT3	13.45	13.56	12.97	12.90	12.95	13.27	13.38	12.76
SkT8	14.45	14.47	13.86	13.84	13.86	14.28	14.38	13.69
SkT9	14.49	14.59	13.93	13.89	13.90	14.38	14.40	13.76
SkT1*	13.44	13.45	12.88	12.87	12.87	13.26	13.25	12.66
SkT3*	13.26	13.27	12.73	12.74	12.74	13.14	13.16	12.56
Skxs20	13.97	14.02	13.43	13.36	13.28	13.74	13.77	13.25
Z-sigma	15.42	15.42	14.77	14.77	14.83	15.24	15.26	14.61
Exp.	14.51	14.55	13.85	13.85	13.60	14.56	14.35	14.49
Error	0.25	0.13	0.20	0.20	0.15	0.20	0.15	0.15

Table A5 Calculated centroid energies (in MeV) for the ISGOR.

ISGOR	^{92}Mo	^{94}Mo	^{96}Mo	^{98}Mo	^{100}Mo	^{90}Zr	^{92}Zr	^{94}Zr
SGII	26.16	26.15	25.74	25.69	25.56	26.07	26.04	25.53
KDE0	27.16	27.15	26.44	26.40	26.31	27.21	27.17	26.59
KDE0v1	26.99	27.01	26.35	26.27	26.11	26.98	26.96	26.18
SKM*	25.92	25.93	25.41	25.35	25.17	25.80	25.79	25.20
Sk255	26.29	26.18	25.45	25.33	25.25	26.08	26.12	25.31
SkI3	29.43	29.30	27.94	27.98	27.90	29.26	29.23	27.78
SkI4	28.33	28.36	27.28	27.20	27.18	28.23	28.28	27.43
SkI5	28.92	28.91	27.87	27.95	27.86	28.88	28.90	27.91
SV-bas	25.38	25.27	24.67	24.53	24.45	25.29	25.23	24.58
SV-min	24.83	24.76	24.23	24.09	23.91	24.73	24.60	24.03
SV-sym32	25.33	25.20	24.58	24.46	24.31	25.19	25.10	24.43
SV-m56-O	29.61	29.70	28.28	28.31	28.34	29.41	29.55	28.17
SV-m64-O	28.47	28.43	27.65	27.60	27.51	28.28	28.38	27.43
SLy4	27.18	27.18	26.48	26.47	26.30	27.08	27.05	26.46
SLy5	27.15	27.17	26.50	26.47	26.36	27.14	27.12	26.32
SLy6	27.33	27.33	26.75	26.77	26.65	27.27	27.27	26.49
SkMP	27.60	27.59	26.93	26.91	26.83	27.52	27.55	26.81
SKO	25.14	25.08	24.45	24.26	24.50	25.24	25.17	24.55
SKO`	25.62	25.57	24.88	24.68	24.56	25.52	25.45	24.70
LNS	26.93	26.90	26.34	26.30	26.13	26.88	26.84	26.13
MSL0	26.30	26.27	25.63	25.54	25.39	26.08	26.10	25.47
NRAPR	27.47	27.45	26.42	26.32	26.30	27.36	27.35	26.81
SQMC650	26.45	26.46	25.89	25.90	25.74	26.48	26.44	25.77
SQMC700	27.22	27.24	26.65	26.64	26.43	27.26	27.20	26.46
SkT1	24.48	24.19	23.72	23.53	23.40	24.16	24.05	23.52
SkT2	24.29	24.22	23.80	23.62	23.45	24.15	24.08	23.58
SkT3	24.40	24.29	23.84	23.63	23.51	24.28	24.16	23.66
SkT8	26.09	26.02	25.43	25.29	25.20	25.94	25.95	25.23
SkT9	25.97	25.92	25.34	25.22	25.13	25.77	25.85	25.17
SkT1*	24.23	24.17	23.65	23.45	23.34	24.12	24.01	23.47
SkT3*	24.14	24.04	23.50	23.28	23.20	24.12	24.02	23.41
Skxs20	24.38	24.34	23.89	23.75	23.48	24.39	24.32	23.74
Z-sigma	26.81	26.82	26.28	26.25	26.17	26.89	26.89	26.24
Exp.	21.80	24.60	21.40	21.50	21.51	23.10	23.90	23.6
Error	0.30	0.46	0.30	0.30	0.30	0.30	0.30	0.30

Table A6 Calculated centroid energies (in MeV) for the IVGMR.

IVGMR	^{92}Mo	^{94}Mo	^{96}Mo	^{98}Mo	^{100}Mo	^{90}Zr	^{92}Zr	^{94}Zr
SGII	31.71	31.56	30.86	30.73	30.71	31.71	31.54	30.83
KDE0	31.77	31.57	30.83	30.67	30.77	31.72	31.55	30.76
KDE0v1	31.41	31.27	30.52	30.35	30.44	31.36	31.22	30.44
SKM*	31.84	31.70	31.08	30.93	30.91	31.82	31.68	31.05
Sk255	33.70	33.57	32.67	32.50	32.51	33.60	33.48	32.57
SkI3	32.62	32.50	31.44	31.37	31.38	32.36	32.23	31.18
SkI4	33.97	33.93	32.64	32.54	32.65	33.75	33.69	32.37
SkI5	32.07	31.98	30.85	30.75	30.79	31.84	31.73	30.57
SV-bas	32.59	32.45	31.77	31.59	31.59	32.64	32.48	31.76
SV-min	30.06	29.89	29.29	29.11	29.06	30.11	29.94	29.32
SV-sym32	32.76	32.63	31.89	31.74	31.66	32.79	32.63	31.88
SV-m56-O	36.75	36.70	34.92	34.92	35.11	36.53	36.65	34.94
SV-m64-O	35.94	35.93	34.62	34.60	34.77	35.77	35.78	34.43
SLy4	30.07	29.89	29.31	29.15	29.26	30.01	29.87	29.22
SLy5	30.16	30.00	29.41	29.25	29.36	30.12	29.97	29.32
SLy6	30.97	30.79	30.11	29.97	30.02	30.90	30.73	30.00
SkMP	33.37	33.23	32.32	32.29	32.24	33.18	33.03	32.15
SKO	27.82	27.68	27.03	26.85	27.03	27.97	27.83	27.18
SKO`	30.93	30.78	30.02	29.84	29.84	30.89	30.74	29.97
LNS	32.38	32.23	31.54	31.43	31.40	32.36	32.18	31.49
MSL0	31.06	30.97	30.29	30.16	30.15	31.06	30.95	30.25
NRAPR	33.71	33.52	32.43	32.27	32.44	33.62	33.46	32.26
SQMC650	32.79	32.67	32.00	31.92	31.84	32.69	32.60	31.90
SQMC700	33.95	33.82	32.93	32.81	32.78	33.87	33.76	32.85
SkT1	28.27	28.14	27.70	27.50	27.48	28.33	28.19	27.69
SkT2	28.28	28.13	27.68	27.51	27.48	28.33	28.20	27.72
SkT3	28.70	28.55	28.06	27.87	27.80	28.76	28.61	28.05
SkT8	30.21	30.05	29.43	29.26	29.30	30.19	30.07	29.40
SkT9	30.05	29.89	29.31	29.13	29.19	30.06	29.94	29.32
SkT1*	28.17	28.03	27.56	27.39	27.39	28.21	28.06	27.55
SkT3*	28.54	28.38	27.85	27.68	27.68	28.59	28.45	27.87
Skxs20	29.75	29.49	28.96	28.78	28.68	29.67	29.49	28.96
Z-sigma	33.71	33.49	32.56	32.39	32.61	33.73	33.56	32.63
Exp. Error								

Table A7 Calculated centroid energies (in MeV) for the IVGDR.

IVGDR	^{92}Mo	^{94}Mo	^{96}Mo	^{98}Mo	^{100}Mo	^{90}Zr	^{92}Zr	^{94}Zr
SGII	16.69	16.58	16.06	16.02	15.88	16.78	16.65	16.09
KDE0	17.05	16.96	16.31	16.24	16.14	17.11	16.99	16.24
KDE0v1	16.75	16.63	16.04	15.95	15.87	16.81	16.68	15.91
SKM*	16.97	16.89	16.39	16.33	16.18	17.05	16.93	16.35
Sk255	17.28	17.20	16.45	16.39	16.32	17.29	17.19	16.26
SkI3	16.37	16.29	15.43	15.42	15.28	16.32	16.22	15.35
SkI4	17.44	17.33	16.24	16.19	16.11	17.43	17.32	16.17
SkI5	15.53	15.45	14.49	14.46	14.42	15.48	15.35	14.41
SV-bas	17.32	17.24	16.67	16.60	16.45	17.45	17.29	16.67
SV-min	15.56	15.48	14.95	14.85	14.73	15.67	15.54	14.90
SV-sym32	17.05	16.94	16.34	16.24	16.11	17.12	16.97	16.28
SV-m56-O	19.37	19.26	17.94	17.87	17.80	19.37	19.21	17.87
SV-m64-O	19.21	19.09	18.10	18.02	17.89	19.29	19.11	18.09
SLy4	16.15	16.08	15.52	15.44	15.39	16.23	16.09	15.21
SLy5	16.14	16.06	15.48	15.45	15.32	16.21	16.06	15.32
SLy6	16.49	16.37	15.82	15.76	15.65	16.56	16.42	15.83
SkMP	17.36	17.28	16.59	16.57	16.42	17.35	17.22	16.52
SKO	13.82	13.74	13.07	13.04	13.10	13.98	13.84	13.29
SKO`	15.74	15.67	14.93	14.84	14.76	15.80	15.67	14.84
LNS	17.15	17.04	16.50	16.49	16.36	17.21	17.07	16.30
MSL0	16.11	16.02	15.42	15.39	15.30	16.15	16.04	15.34
NRAPR	17.89	17.78	16.93	16.85	16.82	17.99	17.82	16.89
SQMC650	17.84	17.77	17.18	17.14	16.98	17.89	17.78	17.19
SQMC700	18.25	18.16	17.45	17.44	17.27	18.28	18.15	17.42
SkT1	14.54	14.51	14.03	13.94	13.85	14.66	14.52	14.05
SkT2	14.60	14.48	14.04	13.97	13.89	14.67	14.54	14.05
SkT3	14.69	14.60	14.08	13.99	13.96	14.78	14.65	14.12
SkT8	16.00	15.88	15.35	15.28	15.18	16.10	15.96	15.03
SkT9	15.96	15.87	15.31	15.25	15.16	16.06	15.94	15.22
SkT1*	14.52	14.42	13.93	13.89	13.81	14.61	14.49	13.99
SkT3*	14.57	14.50	13.99	13.89	13.82	14.70	14.60	14.02
Skxs20	15.49	15.38	14.87	14.79	14.67	15.52	15.40	14.86
Z-sigma	19.12	19.02	18.41	18.33	18.21	19.29	19.14	18.44
Exp.	16.90	16.40	16.20	15.80	15.70	16.83	16.27	16.2
Error	0.10	0.10	0.10	0.10	0.10	0.04	0.04	0.04

Table A8 Calculated centroid energies (in MeV) for the IVGQR.

IVGQR	^{92}Mo	^{94}Mo	^{96}Mo	^{98}Mo	^{100}Mo	^{90}Zr	^{92}Zr	^{94}Zr
SGII	27.39	27.24	26.77	26.52	26.33	27.48	27.30	26.97
KDE0	27.78	27.61	27.18	27.02	26.85	27.78	27.61	27.19
KDE0v1	27.25	27.08	26.70	26.51	26.38	27.28	27.08	26.63
SKM*	27.36	27.22	26.74	26.69	26.35	27.39	27.24	26.96
Sk255	27.50	27.35	26.96	26.78	26.65	27.50	27.34	26.91
SkI3	27.80	27.70	27.04	26.92	26.71	27.63	27.54	26.83
SkI4	28.69	28.54	27.72	27.57	27.41	28.62	28.39	27.56
SkI5	26.81	26.65	25.98	25.86	25.72	26.66	26.48	25.72
SV-bas	27.58	27.41	27.11	26.92	26.71	27.67	27.47	27.14
SV-min	25.18	25.03	24.71	24.55	24.35	25.27	25.10	24.77
SV-sym32	27.12	26.95	26.62	26.43	26.23	27.16	27.00	26.62
SV-m56-O	31.93	31.72	30.69	30.55	30.44	32.08	31.54	30.53
SV-m64-O	31.26	31.07	30.30	30.13	29.97	31.39	30.98	30.24
SLy4	26.65	26.47	26.14	25.98	25.87	26.69	26.52	26.10
SLy5	26.67	26.50	26.16	25.97	25.83	26.69	26.50	26.11
SLy6	27.23	27.05	26.65	26.46	26.26	27.27	27.07	26.67
SkMP	28.57	28.41	27.96	27.82	27.54	28.44	28.28	27.85
SKO	23.69	23.55	23.21	23.01	22.76	23.89	23.74	23.36
SKO`	25.39	25.24	24.81	24.62	24.51	25.43	25.28	24.82
LNS	27.85	27.70	27.30	27.15	26.96	27.92	27.73	27.35
MSL0	26.32	26.19	25.86	25.71	25.56	26.34	26.21	25.85
NRAPR	28.91	28.74	28.21	28.04	28.01	28.99	28.78	28.25
SQMC650	28.32	28.17	27.81	27.68	27.50	28.31	28.16	27.87
SQMC700	29.19	29.02	28.60	28.44	28.17	29.19	29.00	28.58
SkT1	23.64	23.48	23.26	23.08	22.94	23.71	23.56	23.30
SkT2	23.64	23.51	23.29	23.13	22.97	23.72	23.57	23.30
SkT3	23.85	23.71	23.42	23.26	23.13	23.93	23.78	23.47
SkT8	26.06	25.91	25.58	25.39	25.28	26.14	25.98	25.60
SkT9	25.98	25.84	25.53	25.34	25.22	26.06	25.90	25.54
SkT1*	23.57	23.45	23.21	23.02	22.89	23.68	23.54	23.24
SkT3*	23.68	23.54	23.24	23.09	22.96	23.83	23.67	23.36
Skxs20	24.74	24.57	24.32	24.15	23.93	24.75	24.59	24.30
Z-sigma	30.53	30.33	30.03	29.86	29.66	30.68	30.49	30.13
Exp. Error								

Table A9 Calculated centroid energies (in MeV) for the IVGOR.

IVGOR	^{92}Mo	^{94}Mo	^{96}Mo	^{98}Mo	^{100}Mo	^{90}Zr	^{92}Zr	^{94}Zr
SGII	36.09	35.90	35.54	35.38	34.89	36.12	35.98	35.64
KDE0	36.61	36.32	36.01	35.72	35.55	36.52	36.24	35.94
KDE0v1	36.03	35.81	35.53	35.20	35.05	36.01	35.70	35.39
SKM*	35.61	35.55	35.20	35.10	34.66	35.68	35.53	35.25
Sk255	35.79	35.63	35.22	35.02	34.90	35.78	35.54	35.19
SkI3	36.49	36.55	36.09	36.06	35.94	37.18	36.98	36.92
SkI4	37.43	37.36	36.78	36.67	36.53	37.46	37.19	36.66
SkI5	36.52	36.36	36.14	36.00	36.01	36.52	36.28	35.88
SV-bas	35.79	35.59	35.27	35.16	34.79	35.89	35.71	35.39
SV-min	33.52	33.40	33.01	32.90	32.53	33.63	33.45	33.10
SV-sym32	35.24	35.12	34.74	34.64	34.32	35.35	35.18	34.84
SV-m56-O	39.88	39.64	39.23	39.00	39.15	40.53	39.50	38.95
SV-m64-O	39.79	39.61	39.04	38.87	38.80	40.40	39.44	38.95
SLy4	35.50	35.23	34.97	35.21	35.03	35.44	35.17	34.89
SLy5	35.59	35.32	35.06	35.28	35.07	35.42	35.25	34.95
SLy6	36.27	35.94	35.65	35.40	35.24	36.27	35.94	35.62
SkMP	37.45	37.39	36.85	36.48	36.11	37.30	37.13	36.75
SKO	32.67	32.48	32.01	31.86	31.68	32.94	32.70	32.33
SKO`	33.78	33.63	33.22	32.97	32.84	33.85	33.69	33.27
LNS	36.54	36.37	36.01	35.89	35.60	36.65	36.44	36.05
MSL0	34.87	34.71	34.44	34.21	34.02	34.87	34.71	34.35
NRAPR	37.40	37.07	36.69	36.59	36.61	37.55	37.26	36.84
SQMC650	36.52	36.37	36.08	35.98	35.72	36.49	36.28	36.09
SQMC700	37.69	37.57	37.18	37.13	36.70	37.71	37.50	37.22
SkT1	32.06	31.58	31.30	31.13	30.93	31.88	31.69	31.38
SkT2	31.81	31.60	31.34	31.16	30.94	31.92	31.73	31.42
SkT3	32.07	31.87	31.56	31.38	31.16	32.21	31.99	31.66
SkT8	34.66	34.46	34.10	33.90	33.70	34.66	34.40	34.13
SkT9	34.52	34.38	34.03	33.86	33.59	34.57	34.31	34.02
SkT1*	31.72	31.53	31.25	31.07	30.85	31.83	31.65	31.34
SkT3*	31.83	31.66	31.41	31.12	30.98	32.03	31.86	31.52
Skxs20	32.86	32.68	32.27	32.15	31.87	32.99	32.65	32.33
Z-sigma	38.87	38.67	38.38	38.14	37.98	38.94	38.72	38.34
Exp. Error								

---

[1] N.K. Glendenning, Equation of state from nuclear and astrophysical evidence, Phys. Rev. C. 37 (1988) 2733–2743. doi:10.1103/PhysRevC.37.2733.

[2] J.M. Lattimer, M. Prakash, Neutron star observations: Prognosis for equation of state constraints, Phys. Rep. 442 (2007) 109–165. doi:http://dx.doi.org/10.1016/j.physrep.2007.02.003.

[3] M.N. Harakeh, A. van der (Adriaan) Woude, Giant resonances : fundamental high-frequency modes of nuclear excitation, Oxford University Press, 2001. https://global.oup.com/academic/product/giant-resonances-9780198517337?cc=us&lang=en& (accessed August 20, 2018).

[4] D.H. Youngblood, Y.-W. Lui, Krishichayan, J. Button, G. Bonasera, S. Shlomo, Isoscalar E0, E1, E2, and E3 strength in ^{92,96,98,100}Mo, Phys. Rev. C. 92 (2015) 014318. doi:10.1103/PhysRevC.92.014318.

[5] J. Button, Y.-W. Lui, D.H. Youngblood, X. Chen, G. Bonasera, S. Shlomo, Isoscalar E0 , E1 , E2 , and E3 strength in ^{94}Mo, Phys. Rev. C. 94 (2016) 034315. doi:10.1103/PhysRevC.94.034315.

[6] Krishichayan, Y.-W.W. Lui, J. Button, D.H.H. Youngblood, G. Bonasera, S. Shlomo, Isoscalar giant resonances in ^{90,92,94}Zr, Phys. Rev. C. 92 (2015) 044323. doi:10.1103/PhysRevC.92.044323.

[7] B.K. Agrawal, S. Shlomo, V.K. Au, Determination of the parameters of a Skyrme type effective interaction using the simulated annealing approach, Phys. Rev. C. 72 (2005) 014310. doi:10.1103/PhysRevC.72.014310.

[8] Y.K. Gupta, U. Garg, K.B. Howard, J.T. Matta, M. Şenyiğit, M. Itoh, S. Ando, T. Aoki, A. Uchiyama, S. Adachi, M. Fujiwara, C. Iwamoto, A. Tamii, H. Akimune, C. Kadono, Y. Matsuda, T. Nakahara, T. Furuno, T. Kawabata, M. Tsumura, M.N. Harakeh, N. Kalantar-Nayestanaki, Are there nuclear structure effects on the isoscalar giant monopole resonance and nuclear incompressibility near A ∼ 90?, Phys. Lett. B. 760 (2016) 482–485. doi:10.1016/J.PHYSLETB.2016.07.021.

[9] G. Bonasera, M.R. Anders, S. Shlomo, Giant Resonances in ^{40,48}Ca, ^{68}Ni, ^{90}Zr, ^{116}Sn, ^{144}Sm and ^{208}Pb, Phys. Rev. C. 98 (2018) 054316.

doi:10.1103/PhysRevC.98.054316.

[10] E. Chabanat, P. Bonche, P. Haensel, J. Meyer, R. Schaeffer, A Skyrme parametrization from subnuclear to neutron star densities, Nucl. Phys. A. 627 (1997) 710–746. doi:10.1016/S0375-9474(97)00596-4.

[11] T. Sil, S. Shlomo, B.K. Agrawal, P.-G. Reinhard, Effects of self-consistency violation in Hartree-Fock RPA calculations for nuclear giant resonances revisited, Phys. Rev. C. 73 (2006) 034316. doi:10.1103/PhysRevC.73.034316.

[12] S. Shlomo, A.I. Sanzhur, Isoscalar giant dipole resonance and nuclear matter incompressibility coefficient, Phys. Rev. C. 65 (2002) 044310. doi:10.1103/PhysRevC.65.044310.

[13] B.K. Agrawal, S. Shlomo, A.I. Sanzhur, Self-consistent Hartree-Fock based random phase approximation and the spurious state mixing, Phys. Rev. C. 67 (2003) 034314. doi:10.1103/PhysRevC.67.034314.

[14] M.R. Anders, S. Shlomo, T. Sil, D.H. Youngblood, Y.-W. Lui, Krishichayan, Giant resonances in 40Ca and 48Ca, Phys. Rev. C. 87 (2013) 024303. doi:10.1103/PhysRevC.87.024303.

[15] P.-G. Reinhard, From sum rules to RPA: 1. Nuclei, Ann. Phys. 504 (1992) 632–661. doi:10.1002/andp.19925040805.

[16] B.K. Agrawal, S. Shlomo, Consequences of self-consistency violations in Hartree-Fock random-phase approximation calculations of the nuclear breathing mode energy, Phys. Rev. C. 70 (2004) 014308. doi:10.1103/PhysRevC.70.014308.

[17] I. Hamamoto, H. Sagawa, X.Z. Zhang, Single-particle and collective properties of drip-line nuclei, Phys. Rev. C. 53 (1996) 765–774. doi:10.1103/PhysRevC.53.765.

[18] J.A. Maruhn, P.-G. Reinhard, P.D. Stevenson, A.S. Umar, The TDHF code Sky3D, Comput. Phys. Commun. 185 (2014) 2195–2216. doi:10.1016/J.CPC.2014.04.008.

[19] L.-G. Cao, H. Sagawa, G. Colò, Microscopic study of the isoscalar giant monopole resonance in Cd, Sn, and Pb isotopes, Phys. Rev. C. 86 (2012) 054313. doi:10.1103/PhysRevC.86.054313.

[20] A. Bohr, B.M. Mottelson, Nuclear Structure II, Benjamin, New York, 1975.

[21] S. Shlomo, V.M. Kolomietz, G. Colò, Deducing the nuclear-matter incompressibility coefficient from data on isoscalar compression modes, Eur. Phys.

J. A. 30 (2006) 23–30. doi:10.1140/epja/i2006-10100-3.

[22] J.P. Blaizot, Nuclear compressibilities, Phys. Rep. 64 (1980) 171–248. doi:http://dx.doi.org/10.1016/0370-1573(80)90001-0.

[23] S. Shlomo, D.H. Youngblood, Nuclear matter compressibility from isoscalar giant monopole resonance, Phys. Rev. C. 47 (1993) 529–536. doi:10.1103/PhysRevC.47.529.

[24] S. Shlomo, Compression modes and the nuclear matter incompressibility coefficient, Pramana. 57 (2001) 557–570. doi:10.1007/s12043-001-0062-4.

[25] Y.-W. Lui, D.H. Youngblood, S. Shlomo, X. Chen, Y. Tokimoto, Krishichayan, M. Anders, J. Button, Isoscalar giant resonances in Ca 48, Phys. Rev. C. 83 (2011) 044327. doi:10.1103/PhysRevC.83.044327.

[26] H. Beil, R. Bergère, P. Carlos, A. Leprêtre, A. De Miniac, A. Veyssière, A study of the photoneutron contribution to the giant dipole resonance in doubly even Mo isotopes, Nucl. Phys. A. 227 (1974) 427. doi:10.1016/0375-9474(74)90769-6.

[27] B.L. Berman, J.T. Caldwell, R.R. Harvey, M.A. Kelly, R.L. Bramblett, S.C. Fultz, Photoneutron Cross Sections for ^{90}Zr, ^{91}Zr, ^{92}Zr, ^{94}Zr, and ^{89}Y, Phys. Rev. 162 (1967) 1098–1111. doi:10.1103/PhysRev.162.1098.

[28] Y.K. Gupta, K.B. Howard, U. Garg, J.T. Matta, M. Şenyiğit, M. Itoh, S. Ando, T. Aoki, A. Uchiyama, S. Adachi, M. Fujiwara, C. Iwamoto, A. Tamii, H. Akimune, C. Kadono, Y. Matsuda, T. Nakahara, T. Furuno, T. Kawabata, M. Tsumura, M.N. Harakeh, N. Kalantar-Nayestanaki, Isoscalar giant monopole, dipole, and quadrupole resonances in $^{90,\ 92}$Zr and ^{92}Mo, Phys. Rev. C. 97 (2018) 064323. doi:10.1103/PhysRevC.97.064323.

[29] A. Kolomiets, O. Pochivalov, S. Shlomo, Microscopic description of excitation of nuclear isoscalar giant resonances by inelastic scattering of 240 MeV α particles, Phys. Rev. C. 61 (2000) 034312. doi:10.1103/PhysRevC.61.034312.

[30] S. Kamerdzhiev, J. Speth, G. Tertychny, Extended theory of finite Fermi systems: collective vibrations in closed shell nuclei, Phys. Rep. 393 (2004) 1–86. doi:10.1016/J.PHYSREP.2003.11.001.

[31] V.M. Kolomietz, S. Shlomo, Isoscalar compression modes within fluid dynamic approach, Phys. Rev. C. 61 (2000) 064302. doi:10.1103/PhysRevC.61.064302.

[32] D.C. Fuls, V.M. Kolomietz, S. V. Lukyanov, S. Shlomo, Damping effects on centroid energies of isoscalar compression modes, EPL (Europhysics Lett. 90 (2010) 20006. doi:10.1209/0295-5075/90/20006.

[33] V.M. Kolomietz, S. Shlomo, Nuclear Fermi-liquid drop model, Phys. Rep. 390 (2004) 133–233. doi:10.1016/J.PHYSREP.2003.10.013.

[34] X. Roca-Maza, Y.F. Niu, G. Colò, P.F. Bortignon, Towards a self-consistent dynamical nuclear model, J. Phys. G Nucl. Part. Phys. 44 (2017) 044001. doi:10.1088/1361-6471/aa5669.

[35] Y.F. Niu, G. Colò, E. Vigezzi, Gamow-Teller response and its spreading mechanism in doubly magic nuclei, Phys. Rev. C. 90 (2014) 054328. doi:10.1103/PhysRevC.90.054328.

[36] Y.F. Niu, G. Colò, E. Vigezzi, C.L. Bai, H. Sagawa, Quasiparticle random-phase approximation with quasiparticle-vibration coupling: Application to the Gamow-Teller response of the superfluid nucleus Sn 120, Phys. Rev. C. 94 (2016) 064328. doi:10.1103/PhysRevC.94.064328.

FIGURE CAPTIONS

FIG. 1. The centroid energies, E_{CEN}, obtained from the HF-RPA, are shown as full circles for the isoscalar giant monopole resonance, for the different Skyrme interactions, plotted against the incompressibility coefficient K_{NM}. We plot one isotope per panel. The experimental result is shown by dashed lines (Texas A&M) and solid lines (Osaka). We obtained a strong correlation between the two quantities (C ~ 0.87).

FIG. 2. The difference between the centroid energy [MeV], calculated as $E_{CEN}(^{92}Mo)$ - E_{CEN} ($^{92,94,96,98,100}Mo$) and E_{CEN} (^{90}Zr) – $E_{CEN}(^{90,92,94}Zr)$ in the left and right figures, respectively, is plotted against the asymmetry coefficient I = (N-Z)/A of each isotope, for the isoscalar giant resonances of multipolarity L = 0-3. The experimental result is marked with solid vertical lines, while the results of the HF-RPA are plotted with dots connected by lines to guide the eye.

FIG. 3. Like FIG. 1 but for the isoscalar giant dipole resonance (ISGDR), plotted against K_{NM}. A weak correlation is obtained between the two quantities (C ~ 0.53) due mostly to the already recognized correlation between K_{NM} and m*/m, as shown in Table V of Ref.[9].

FIG. 4. Like FIG. 1 but for the isoscalar giant quadrupole resonance (ISGQR), plotted against m*/m. A strong correlation is obtained between the two quantities (C ~ -0.96).

FIG. 5. Like FIG. 1 but for the isoscalar giant octupole resonance (ISGOR), plotted against m*/m. Strong correlation is obtained between the two quantities (C ~ -0.98).

FIG. 6. Like FIG. 1 but for the isovector giant monopole resonance (IVGMR), plotted against K_{NM}. No correlation is obtained between the two quantities (C ~0.25).

FIG. 7. Like FIG. 1 but for the isovector giant monopole resonance (IVGMR), plotted against J. No correlation is obtained between the two quantities (C ~-0.24).

FIG. 8. The difference between the centroid energy [MeV], calculated as $E_{CEN}(^{92}Mo)$ - E_{CEN} ($^{92,94,96,98,100}Mo$) and E_{CEN} (^{90}Zr) – $E_{CEN}(^{90,92,94}Zr)$ in the left and right figures, respectively, is plotted against the asymmetry term I = (N-Z)/A of each isotope, for the isovector excitation up to L=3. The experimental result (only IVGDR) is marked with solid vertical lines, while the results of the HF-RPA are plotted with dots connected by lines to guide the eye.

FIG. 9. Like FIG. 1 but for the isovector giant dipole resonance (IVGDR), plotted against J. No correlation is obtained between the two quantities (C ~-0.35).

FIG. 10. Like FIG. 1 but for the isovector giant dipole resonance (IVGDR), plotted against κ. Strong correlation is obtained between the two quantities (C ~0.85).

FIG. 11. Like FIG. 1 but for the isovector giant quadrupole resonance (IVGQR), plotted against L. No correlation is obtained between the two quantities (C ~ -0.27).

FIG. 12. Like FIG. 1 but for the isovector giant quadrupole resonance (IVGQR), plotted against m*/m. Medium correlation is obtained between the two quantities (C ~-0.77).

FIG. 13. Like FIG. 1 but for the isovector giant octupole resonance (IVGOR), plotted against K_{sym}. No correlation is obtained between the two quantities (C ~ 0.02).

FIG. 14. Like FIG. 1 but for the isovector giant octupole resonance (IVGOR), plotted against m*/m. Strong correlation is obtained between the two quantities (C ~-0.86).

TABLE I. Experimental data of centroid energy E_{CEN} of the various multipolarities for each nucleus (in MeV). The data for the isoscalar giant resonances in ^{92,96,98,100}Mo isotopes is taken from Ref. [4], in ^{94}Mo from Ref. [5], in ^{90,92,94}Zr from Ref. [6]. The ISGMR data for ^{92}Mo and ^{90,92}Zr from the Osaka group (marked with *) is from Ref. [8]. The data for the isovector giant dipole resonances in ^{92,94,96,98,100}Mo is taken from Ref. [26] and in ^{90,92,94}Zr from Ref. [27].

	L0T0	**L1T0**	**L2T0**	**L3T0**	**L1T1**
^{92}Mo	19.62 (28) 18.20 (13)*	27.60 (50)	14.51 (25)	21.80 (30)	16.90 (.10)
^{94}Mo	17.99 (72)	26.49 (43)	14.55 (13)	24.60 (46)	16.40 (10)
^{96}Mo	16.95 (12)	30.00 (70)	13.85 (20)	21.40 (30)	16.20 (10)
^{98}Mo	16.01 (19)	27.40 (70)	13.85 (20)	21.5 (30)	15.80 (10)
^{100}Mo	16.13 (11)	30.10 (70)	13.60 (15)	21.51 (30)	15.70 (10)
^{90}Zr	17.88 (12) 18.13 (09)*	27.40 (50)	14.56 (20)	23.10 (30)	16.83 (04)
^{92}Zr	18.23 (14) 18.05 (05)*	30.00 (70)	14.35 (15)	23.90 (30)	16.27 (04)
^{94}Zr	16.16 (11)	27.00 (50)	14.49 (15)	23.60 (30)	16.20 (04)

TABLE II. Values of the Pearson linear correlation coefficients determined between the centroid energy of the giant resonances and each nuclear matter property.

	K_{NM}	J	L	K_{sym}	m*/m	κ	$W_0(X_W=1)$
ISGMR	0.87	-0.05	0.25	0.42	-0.51	0.15	0.07
ISGDR	0.53	-0.07	0.12	0.37	-0.91	0.53	0.03
ISGQR	0.37	-0.07	0.15	0.41	-0.96	0.57	0.06
ISGOR	0.38	-0.08	0.13	0.39	-0.98	0.61	0.07
IVGMR	0.25	-0.24	-0.09	0.04	-0.71	0.85	-0.08
IVGDR	0.04	-0.35	-0.39	-0.29	-0.61	0.85	-0.22
IVGQR	0.16	-0.34	-0.27	-0.11	-0.77	0.85	-0.13
IVGOR	0.21	-0.28	-0.18	0.02	-0.86	0.83	-0.07

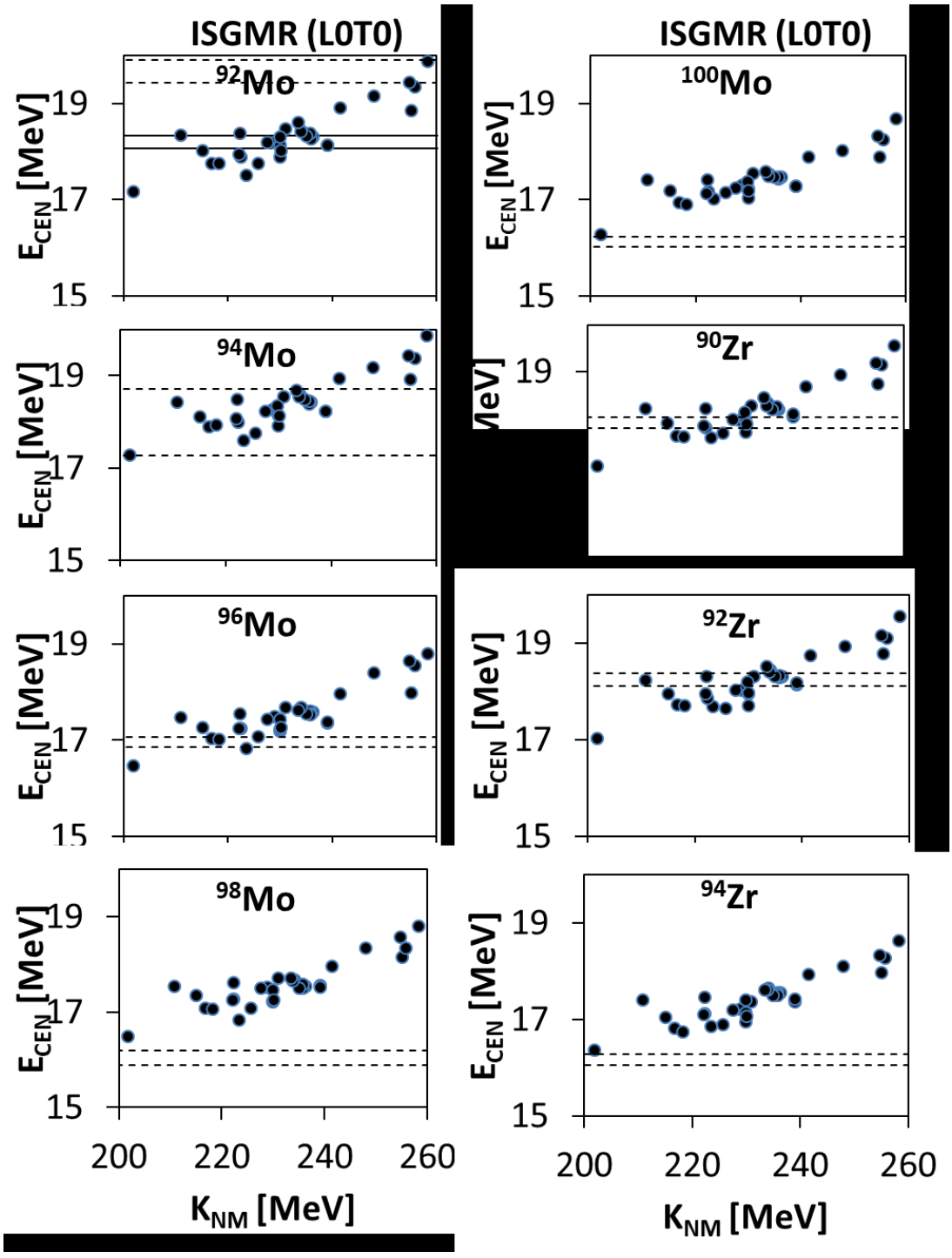

FIG. 1. The centroid energies, E_{CEN}, obtained from the HF-RPA, are shown as full circles for the isoscalar giant monopole resonance, for the different Skyrme interactions, plotted against the incompressibility coefficient K_{NM}. We plot one isotope per panel. The experimental result is shown by dashed lines (Texas A&M) and solid lines (Osaka). We obtained a strong correlation between the two quantities (C ~ 0.87).

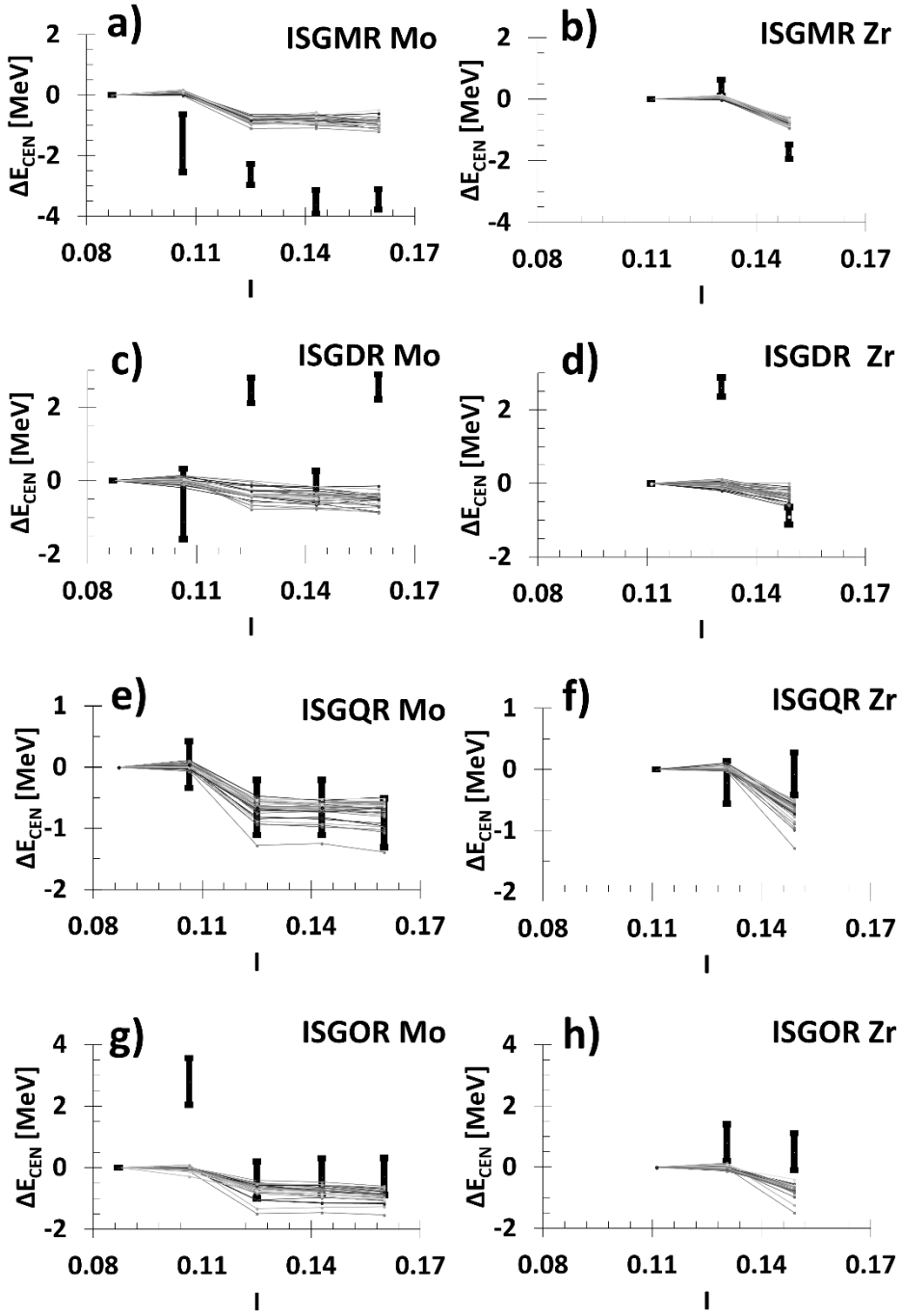

FIG. 2. The difference between the centroid energy [MeV], calculated as $E_{CEN}(^{92}Mo)$ - E_{CEN} ($^{92,94,96,98,100}Mo$) and E_{CEN} (^{90}Zr) – $E_{CEN}(^{90,92,94}Zr)$ in the left and right figures, respectively, is plotted against the asymmetry coefficient I = (N-Z)/A of each isotope, for the isoscalar giant resonances of multipolarity L = 0-3. The experimental result is marked with solid vertical lines, while the results of the HF-RPA are plotted with dots connected by lines to guide the eye.

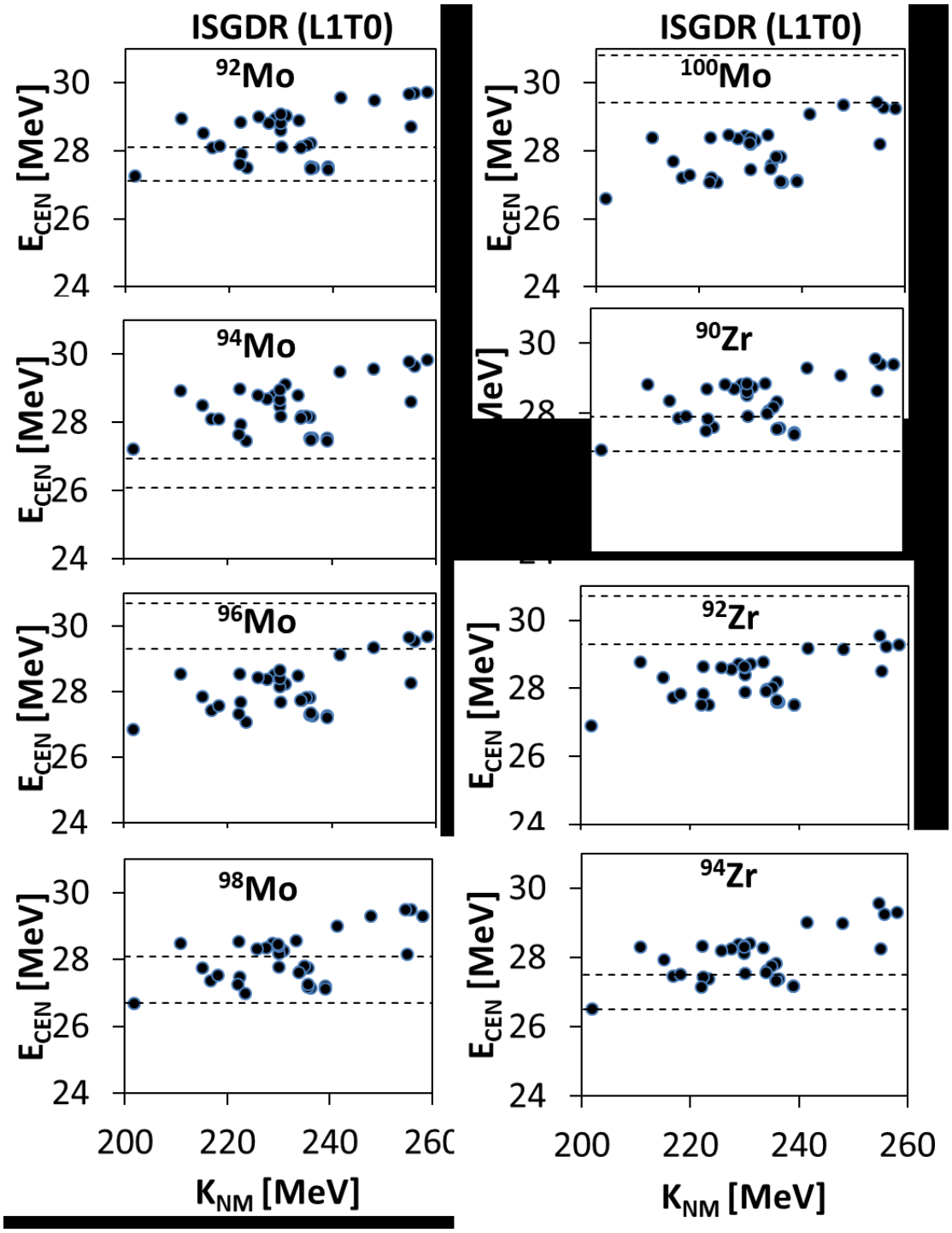

FIG. 3. Like FIG. 1 but for the isoscalar giant dipole resonance (ISGDR), plotted against K_{NM}. A weak correlation is obtained between the two quantities (C ~ 0.53) due mostly to the already recognized correlation between K_{NM} and m*/m, as shown in Table V of Ref.[9].

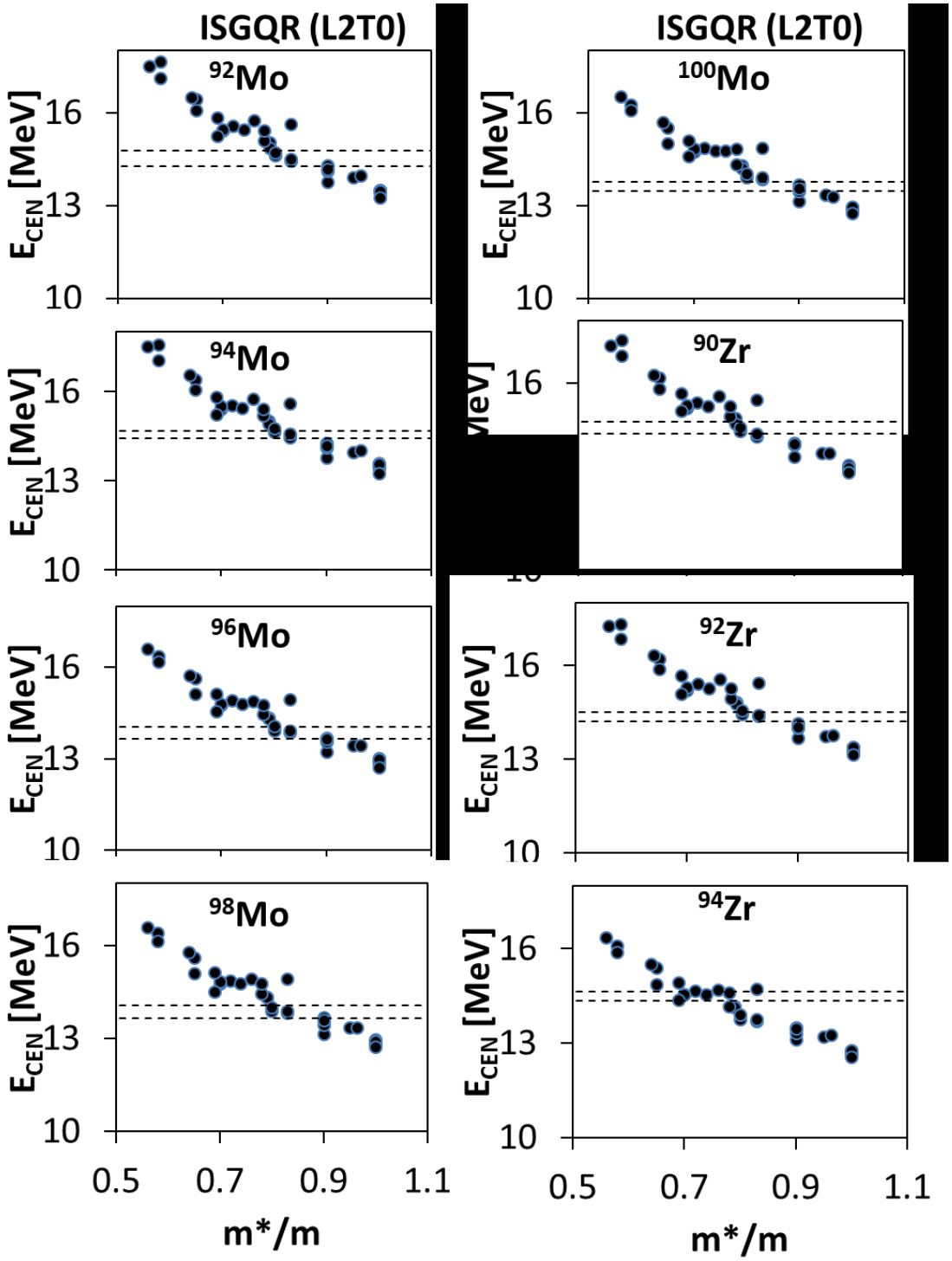

FIG. 4. Like FIG. 1 but for the isoscalar giant quadrupole resonance (ISGQR), plotted against m*/m. A strong correlation is obtained between the two quantities (C ~ -0.96).

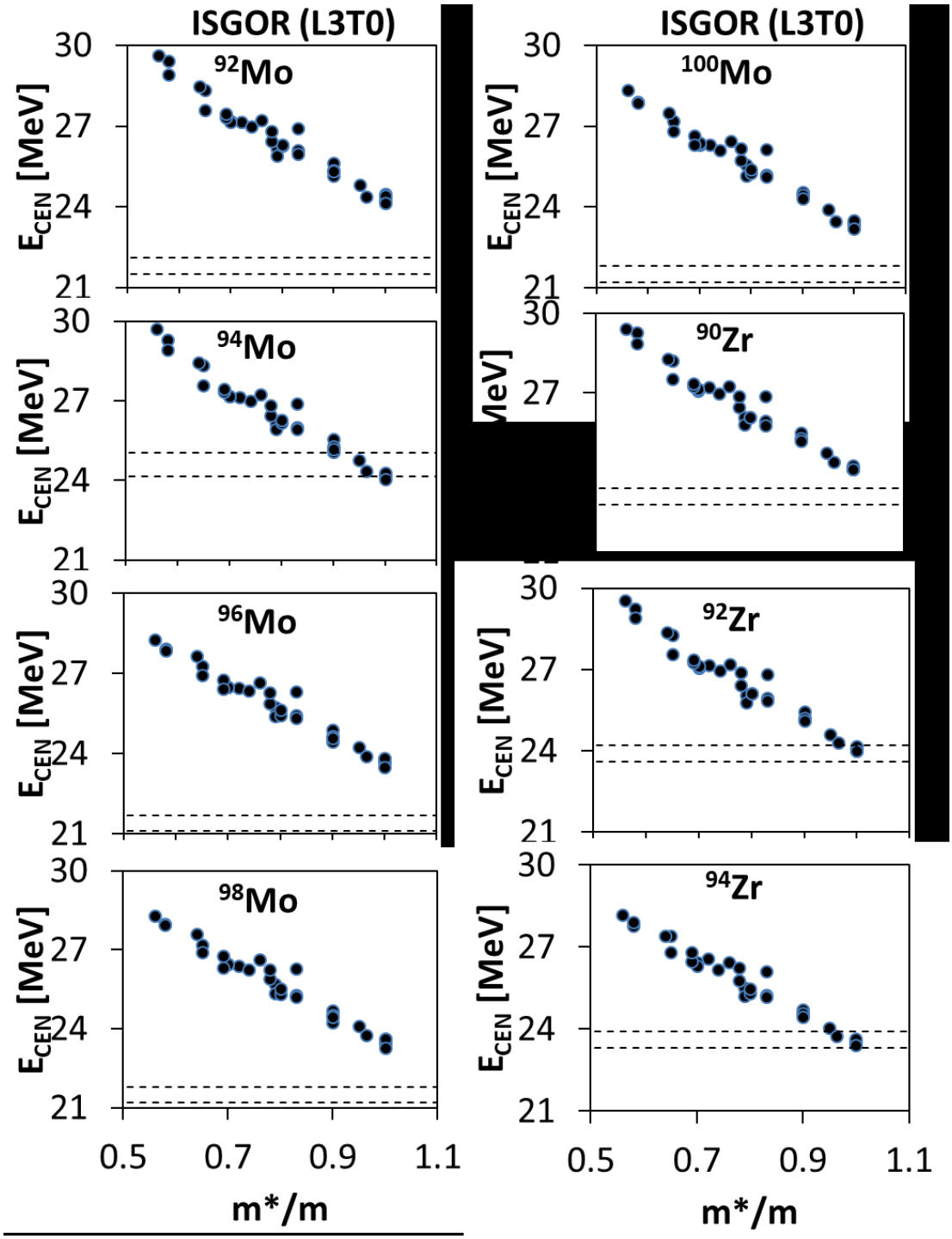

FIG. 5. Like FIG. 1 but for the isoscalar giant octupole resonance (ISGOR), plotted against m*/m. Strong correlation is obtained between the two quantities (C ~ -0.98).

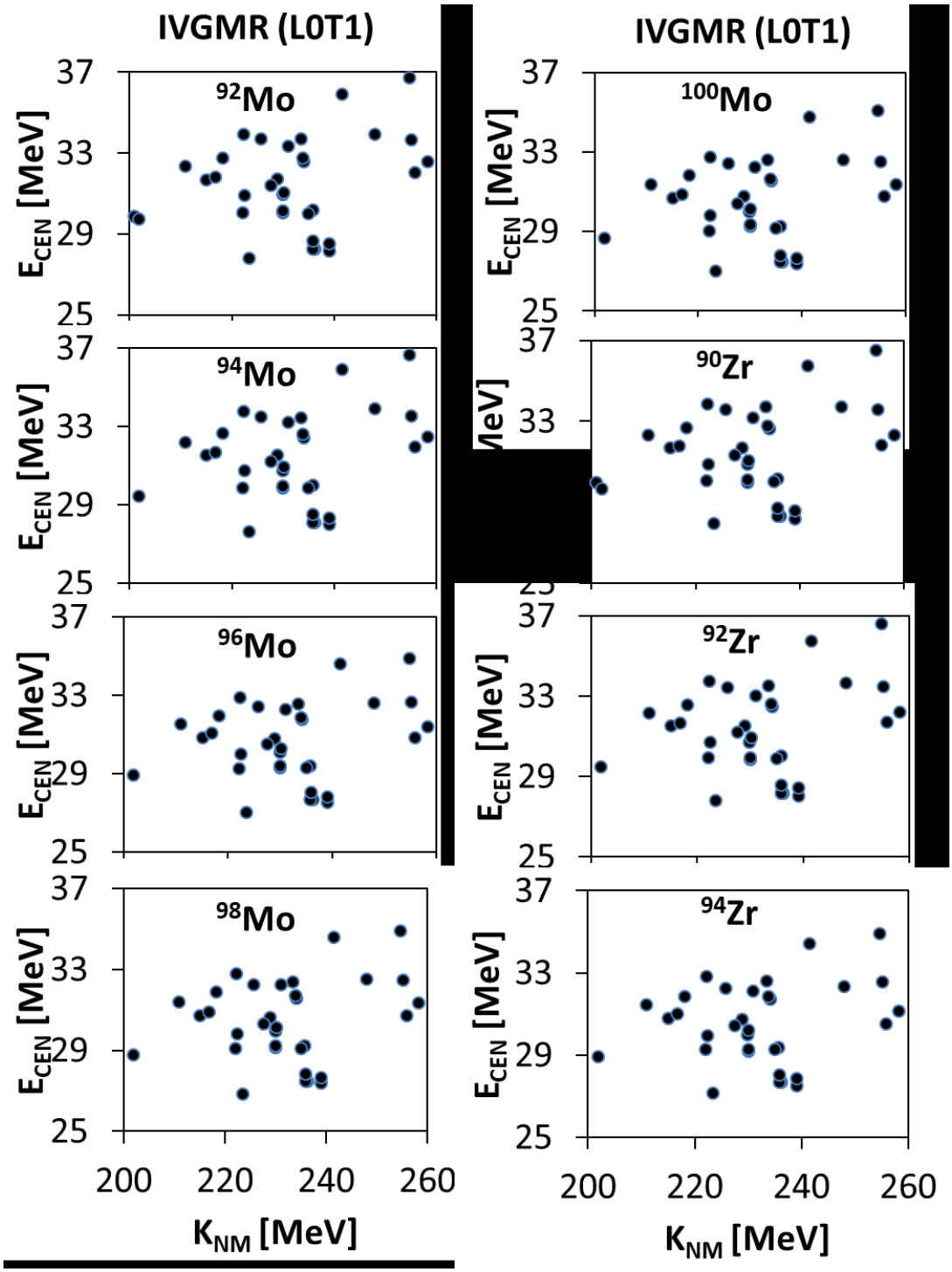

FIG. 6. Like FIG. 1 but for the isovector giant monopole resonance (IVGMR), plotted against K_{NM}. No correlation is obtained between the two quantities (C ~0.25).

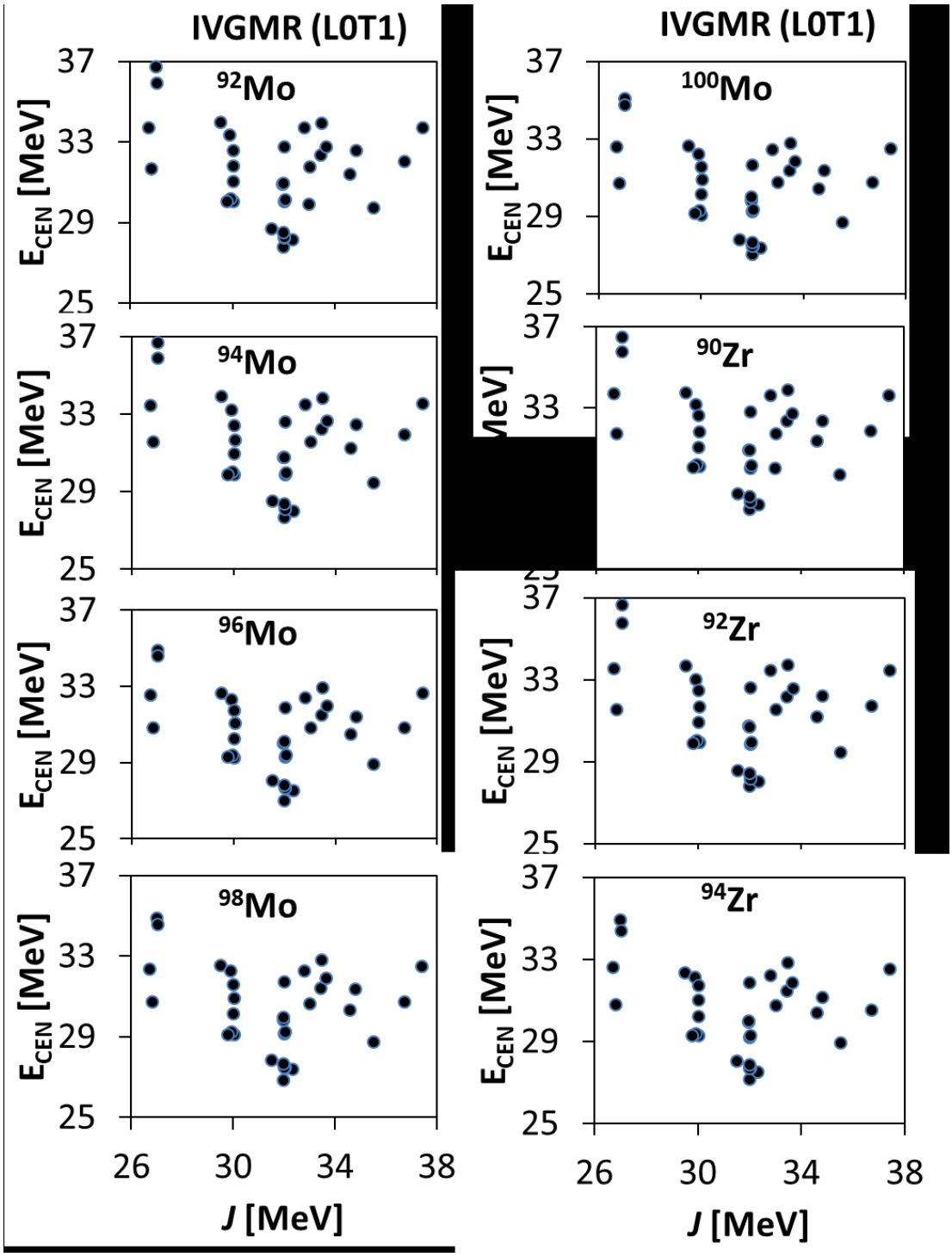

FIG. 7. Like FIG. 1 but for the isovector giant monopole resonance (IVGMR), plotted against J. No correlation is obtained between the two quantities (C ~-0.24).

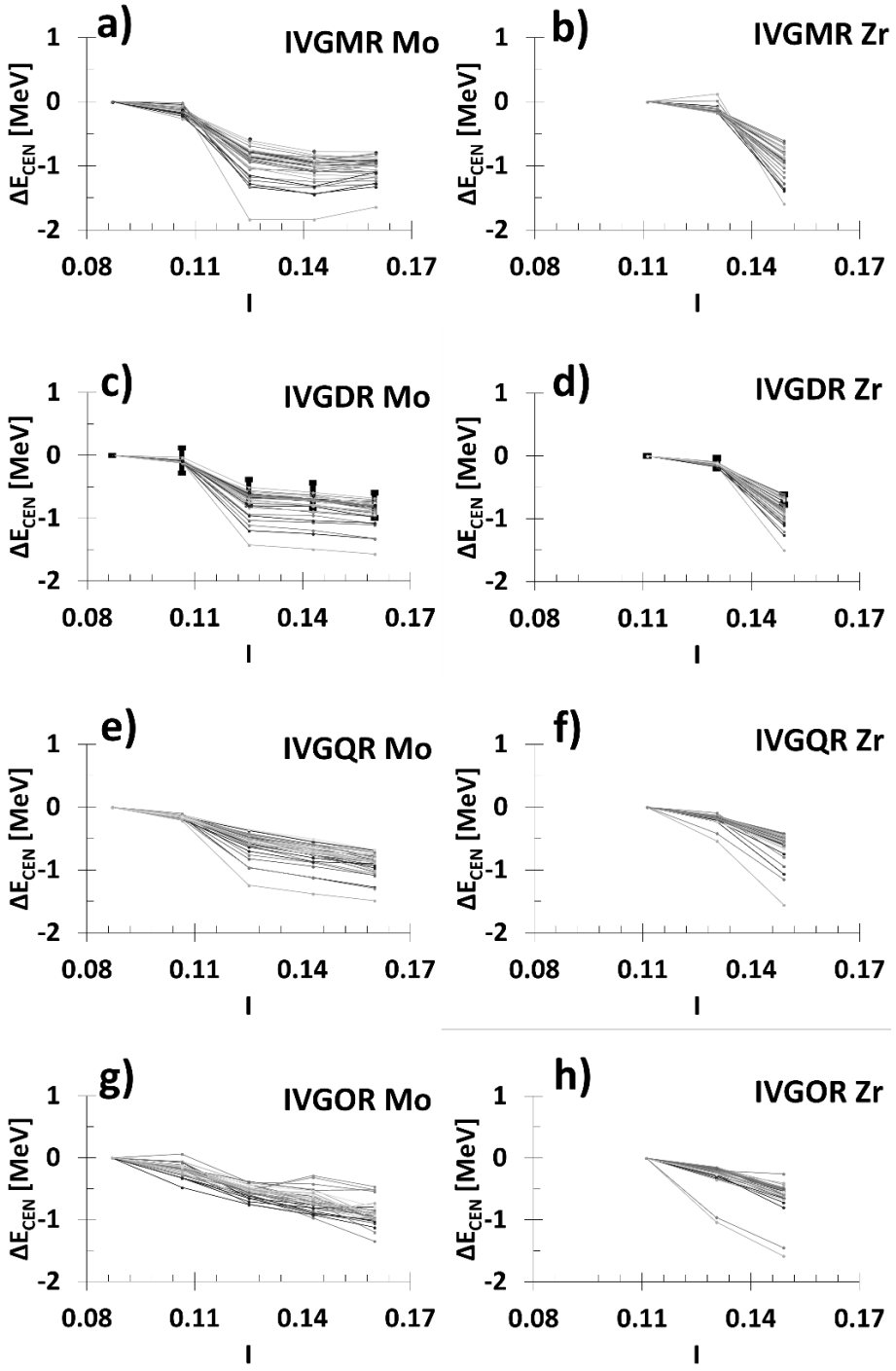

FIG. 8. The difference between the centroid energy [MeV], calculated as $E_{CEN}(^{92}Mo)$ - E_{CEN} ($^{92,94,96,98,100}Mo$) and E_{CEN} (^{90}Zr) – $E_{CEN}(^{90,92,94}Zr)$ in the left and right figures, respectively, is plotted against the asymmetry term I = (N-Z)/A of each isotope, for the isovector excitation up to L=3. The experimental result (only IVGDR) is marked with solid vertical lines, while the results of the HF-RPA are plotted with dots connected by lines to guide the eye.

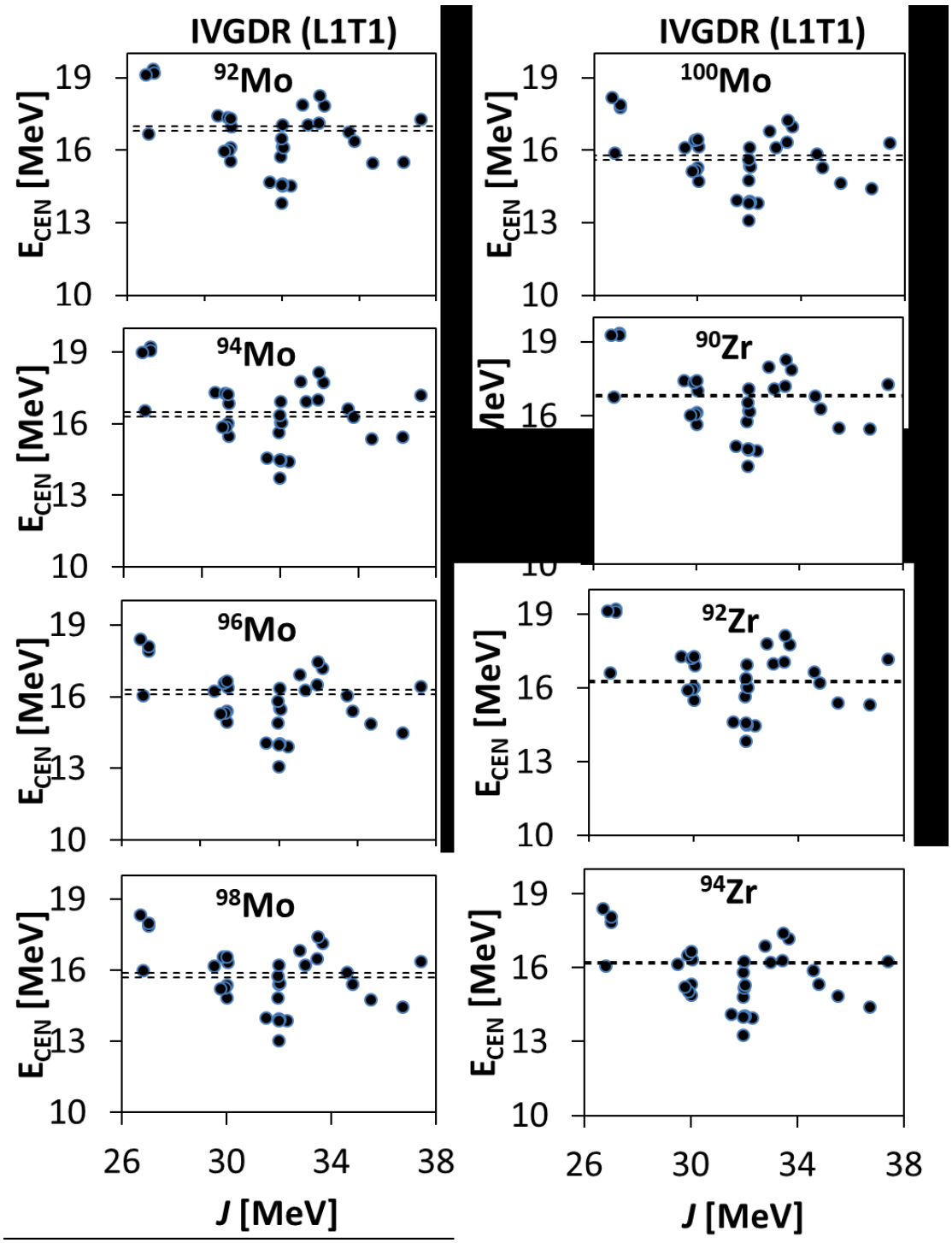

FIG. 9. Like FIG. 1 but for the isovector giant dipole resonance (IVGDR), plotted against J. No correlation is obtained between the two quantities (C ~-0.35).

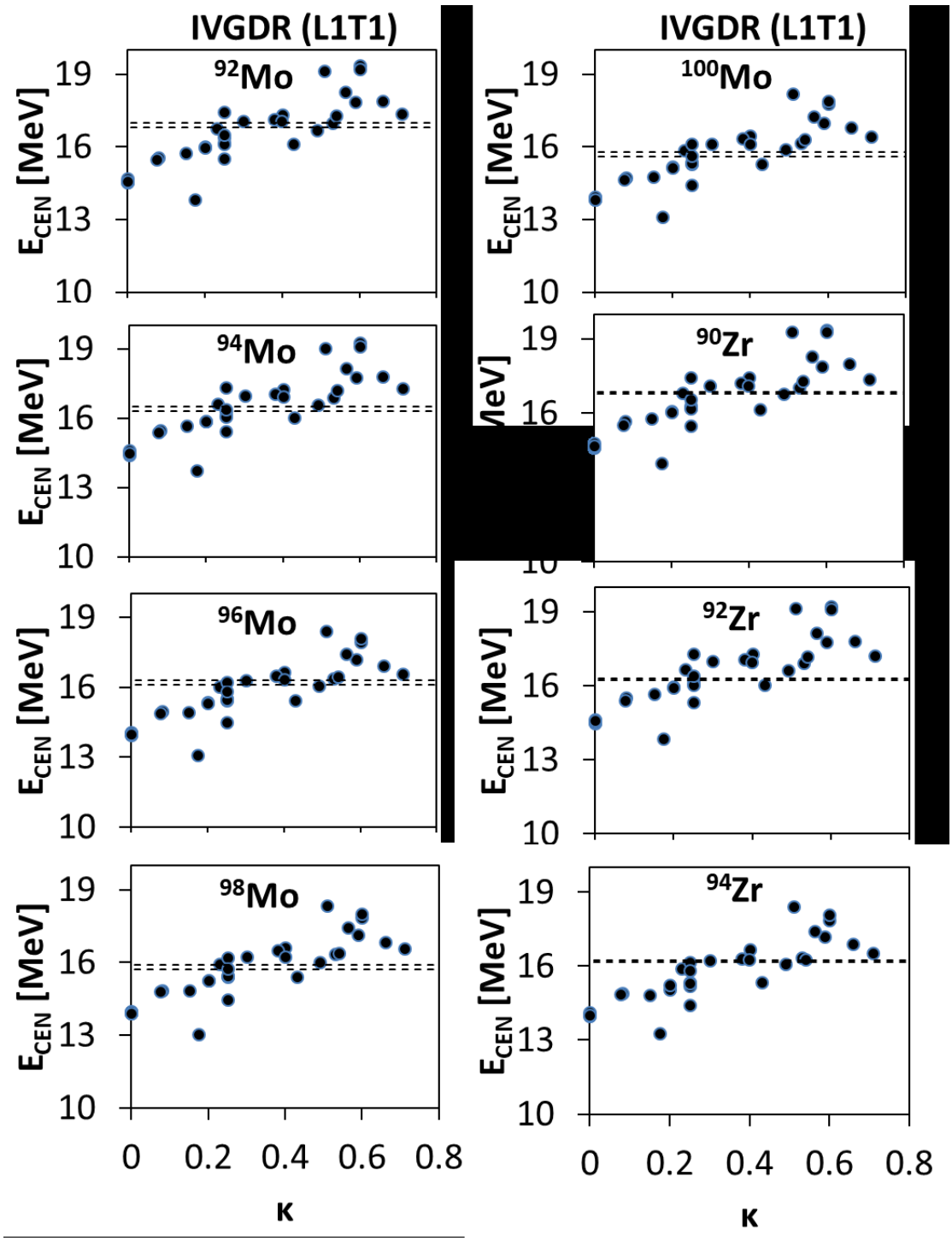

FIG. 10. Like FIG. 1 but for the isovector giant dipole resonance (IVGDR), plotted against κ. Strong correlation is obtained between the two quantities (C ~0.85).

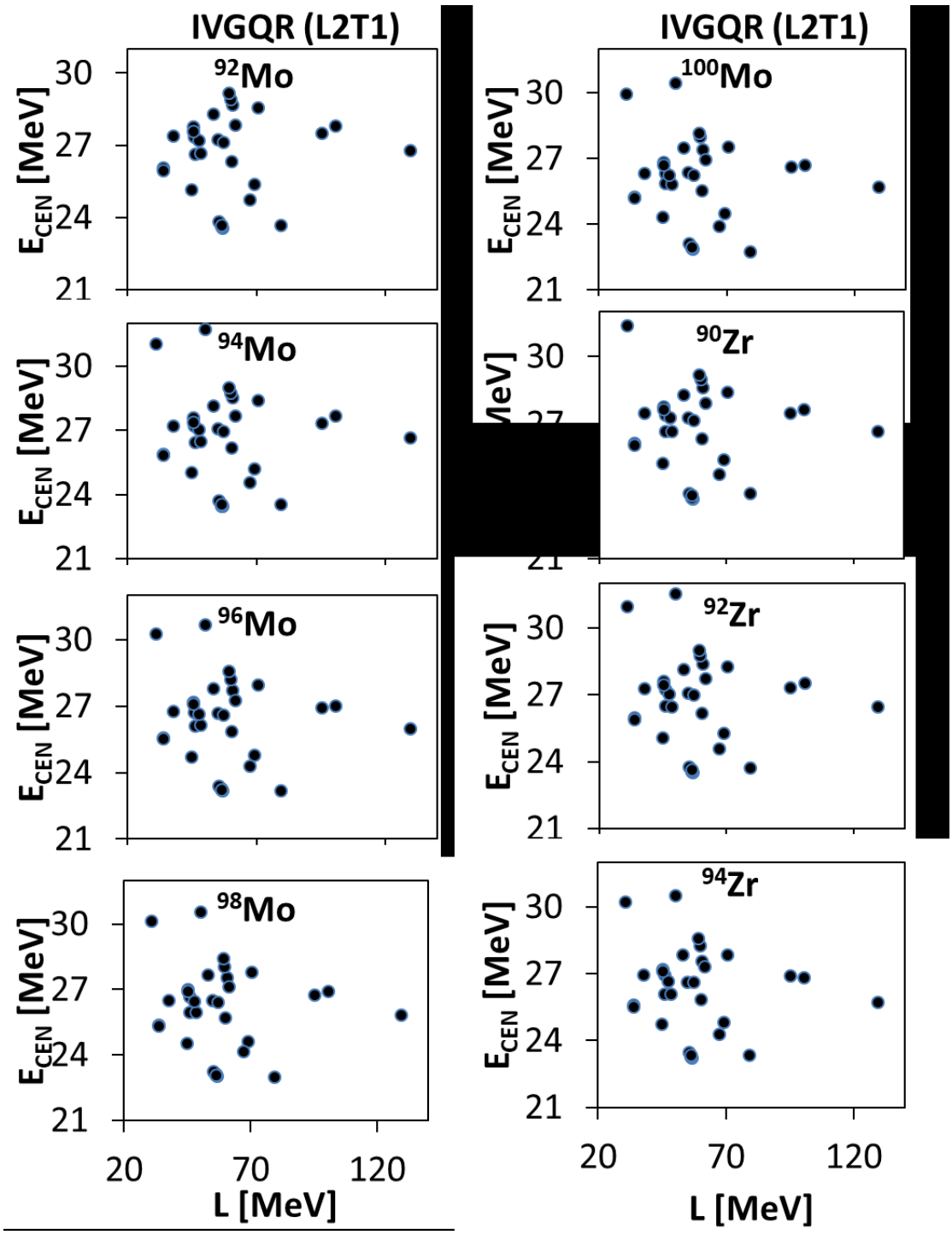

FIG. 11. Like FIG. 1 but for the isovector giant quadrupole resonance (IVGQR), plotted against L. No correlation is obtained between the two quantities (C ~ -0.27).

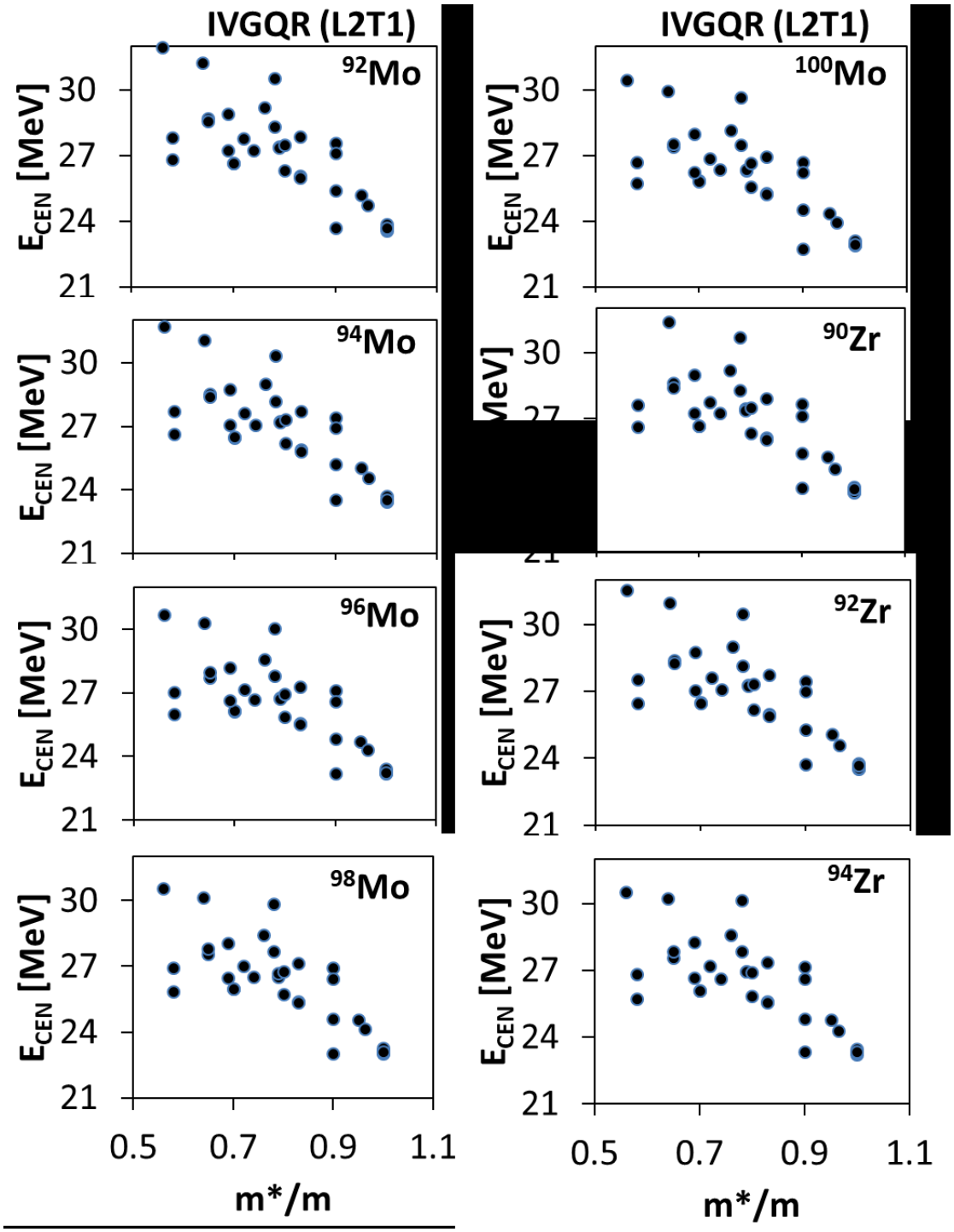

FIG. 12. Like FIG. 1 but for the isovector giant quadrupole resonance (IVGQR), plotted against m*/m. Medium correlation is obtained between the two quantities (C ~-0.77).

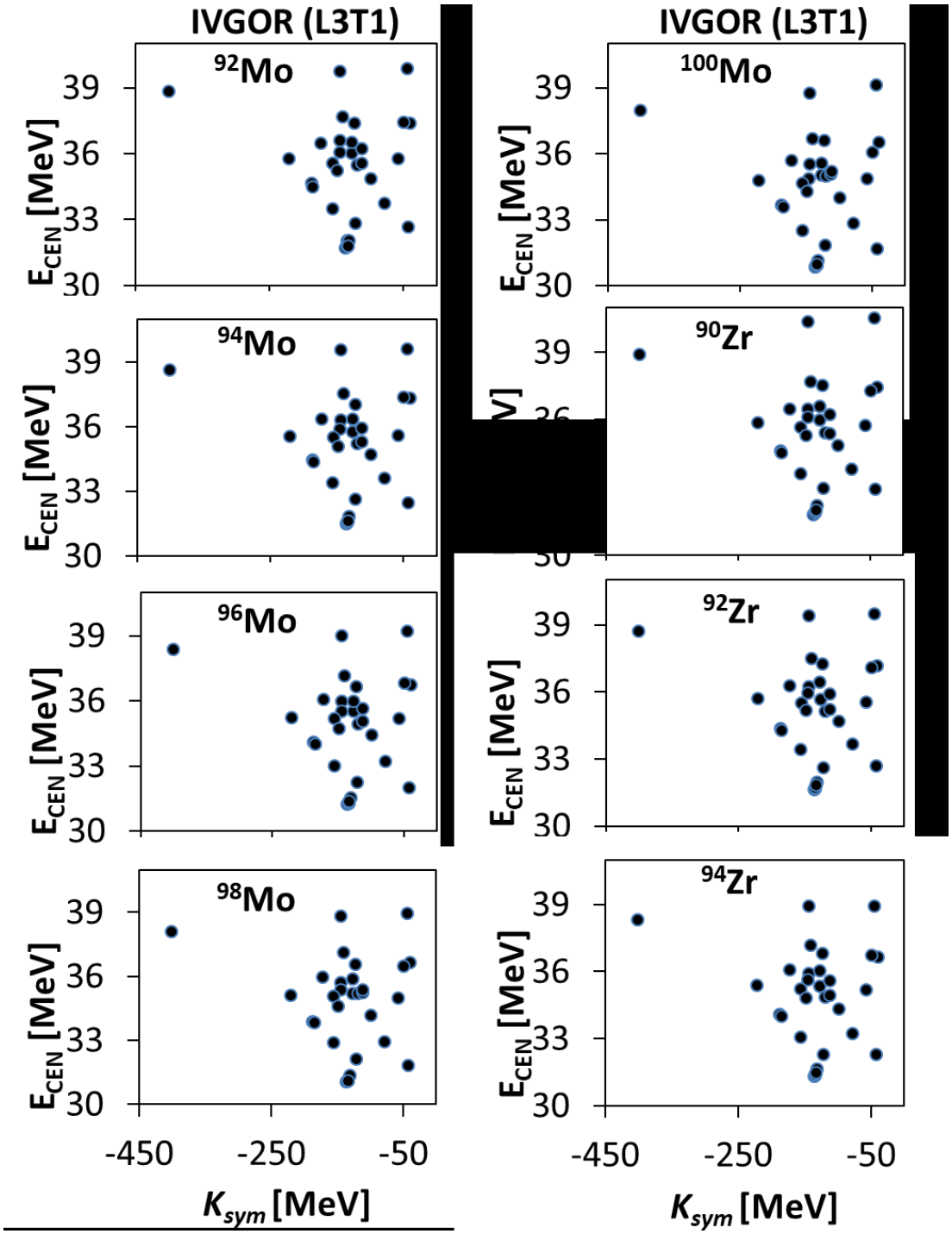

FIG. 13. Like FIG. 1 but for the isovector giant octupole resonance (IVGOR), plotted against K_{sym}. No correlation is obtained between the two quantities (C ~ 0.02).

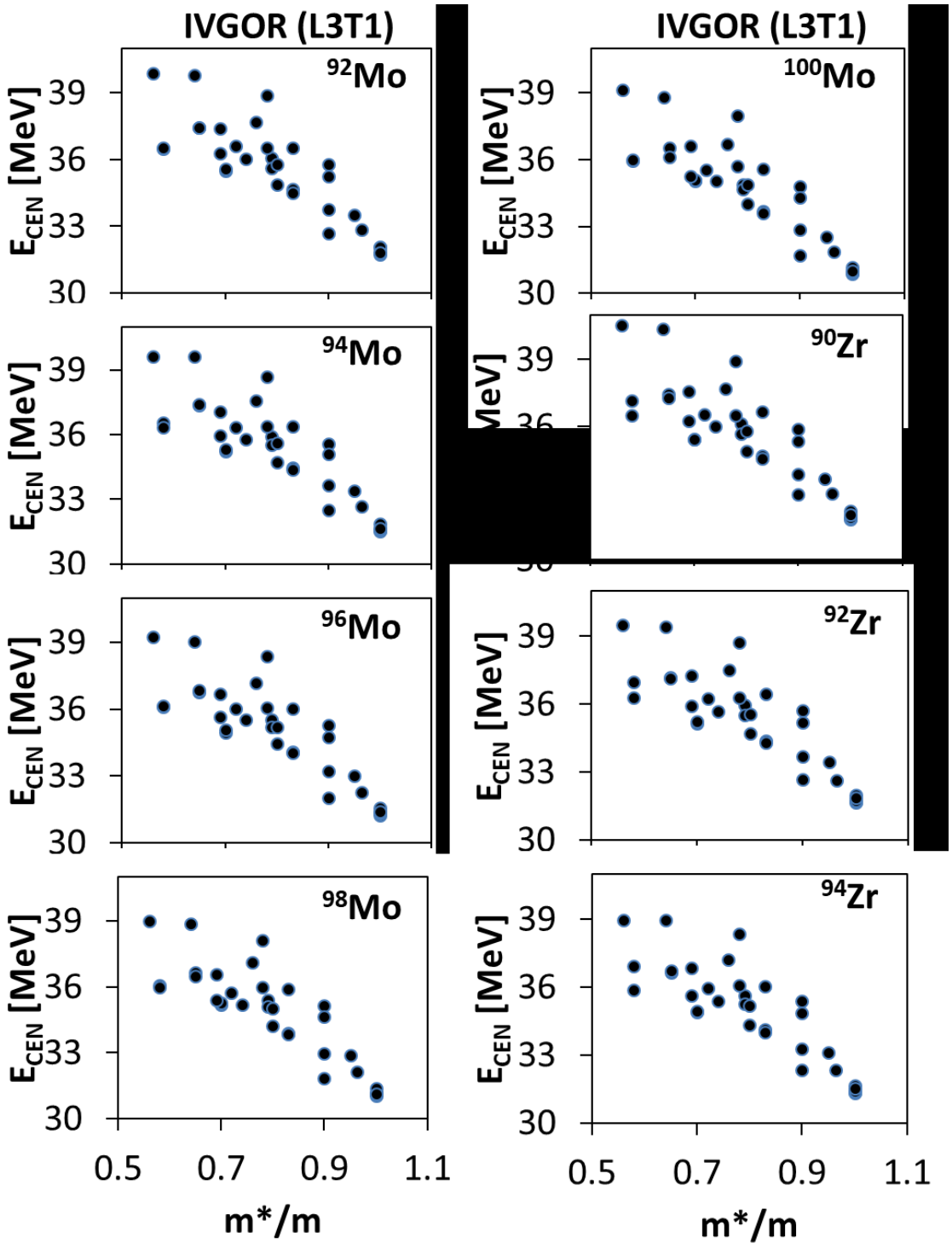

FIG. 14. Like FIG. 1 but for the isovector giant octupole resonance (IVGOR), plotted against m*/m. Strong correlation is obtained between the two quantities (C ~-0.86).